Platinum(II) and Palladium(II) Complexes of Tridentate Hydrazone-Based Ligands as Selective Guanine Quadruplex Binders

Alexander Schmidt, Rweetuparna Guha, Alexander Hepp, Jens Müller*

Westfälische Wilhelms-Universität Münster, Institut für Anorganische und Analytische Chemie, Corrensstraße 28/30, 48149 Münster, Germany.

*Corresponding author: E-mail: mueller.j@uni-muenster.de

Supplementary Material

Table of contents

Fig. S1: CD spectra and melting curves of G4 in the presence of [Pd(**1p**)Cl]Cl S4

Fig. S2: CD spectra and melting curves of G4 in the presence of [Pt(**1p**)Cl]Cl S5

Fig. S3: CD spectra and melting curves of G4 in the presence of [Pd(**1q**)Cl]Cl S6

Fig. S4: CD spectra and melting curves of G4 in the presence of [Pt(**1q**)Cl]Cl S7

Fig. S5: CD spectra and melting curves of G4 in the presence of [Pd(**2p**)Cl] S8

Fig. S6: CD spectra and melting curves of G4 in the presence of [Pd(**2q**)Cl] S9

Fig. S7: CD spectra and melting curves of G4 in the presence of [Pd(**3q**)Cl] S10

Fig. S8: CD spectra and melting curves of G4 in the presence of [Pt(**3q**)Cl] S11

Fig. S9: CD spectra and melting curves of G4 in the presence of [Pt(**4q**)Cl] S12

Fig. S10: CD spectra and melting curves of G4 in the presence of DMSO S13

Fig. S11: CD melting curves of *H-telo* and *c-myc* S14

Fig. S12: Job plots for the binding of [Pd(**1p**)Cl] to G4 ..... S15

Fig. S13: Job plots for the binding of [Pt(**1p**)Cl] to G4 ..... S16

Fig. S14: Job plots for the binding of [Pd(**1q**)Cl] to G4 ..... S17

Fig. S15: Job plots for the binding of [Pt(**1q**)Cl] to G4 ..... S18

Fig. S16: Job plots for the binding of [Pd(**2p**)Cl] to G4 ..... S19

Fig. S17: Job plots for the binding of [Pd(**2q**)Cl] to G4 ..... S20

Fig. S18: Job plots for the binding of [Pd(**3q**)Cl] to G4 ..... S21

Fig. S19: Job plots for the binding of [Pt(**3q**)Cl] to G4 ..... S22

Fig. S20: Job plots for the binding of [Pt(**4q**)Cl] to G4 ..... S23

Fig. S21: FID assay data with [Pd(**1p**)Cl]Cl S24

Fig. S22: FID assay data with [Pt(**1p**)Cl]Cl S25

Fig. S23: FID assay data with [Pd(**1q**)Cl]Cl S26

Fig. S24: FID assay data with [Pt(**1q**)Cl]Cl S27

Fig. S25: FID assay data with [Pd(**2p**)Cl] S28

Fig. S26: FID assay data with [Pd(**2q**)Cl] S29

Fig. S27: FID assay data with [Pd(**3q**)Cl] S30

Fig. S28: FID assay data with [Pt(**3q**)Cl] S31

Fig. S29: FID assay data with [Pt(**4q**)Cl] S32

Fig. S30: Mass spectrum of H(**2q**) S33

Fig. S31: Mass spectrum of H(**3q**) S34

Fig. S32: Mass spectrum of [Pt(**1p**)Cl]Cl S35

Fig. S33: Mass spectrum of [Pd(**1p**)Cl]Cl S35

Fig. S34: Mass spectrum of [Pt(**1q**)Cl]Cl S36

Fig. S35: Mass spectrum of [Pd(**1q**)Cl]Cl S37

Fig. S36: Mass spectrum of [Pd(**2p**)Cl] S38

Fig. S37: Mass spectrum of [Pd(**2q**)Cl] S39

Fig. S38: Mass spectrum of [Pt(**3q**)Cl] S39

Fig. S39: Mass spectrum of [Pd(**3q**)Cl] S40

Fig. S40: Mass spectrum of [Pt(**4q**)Cl] S40

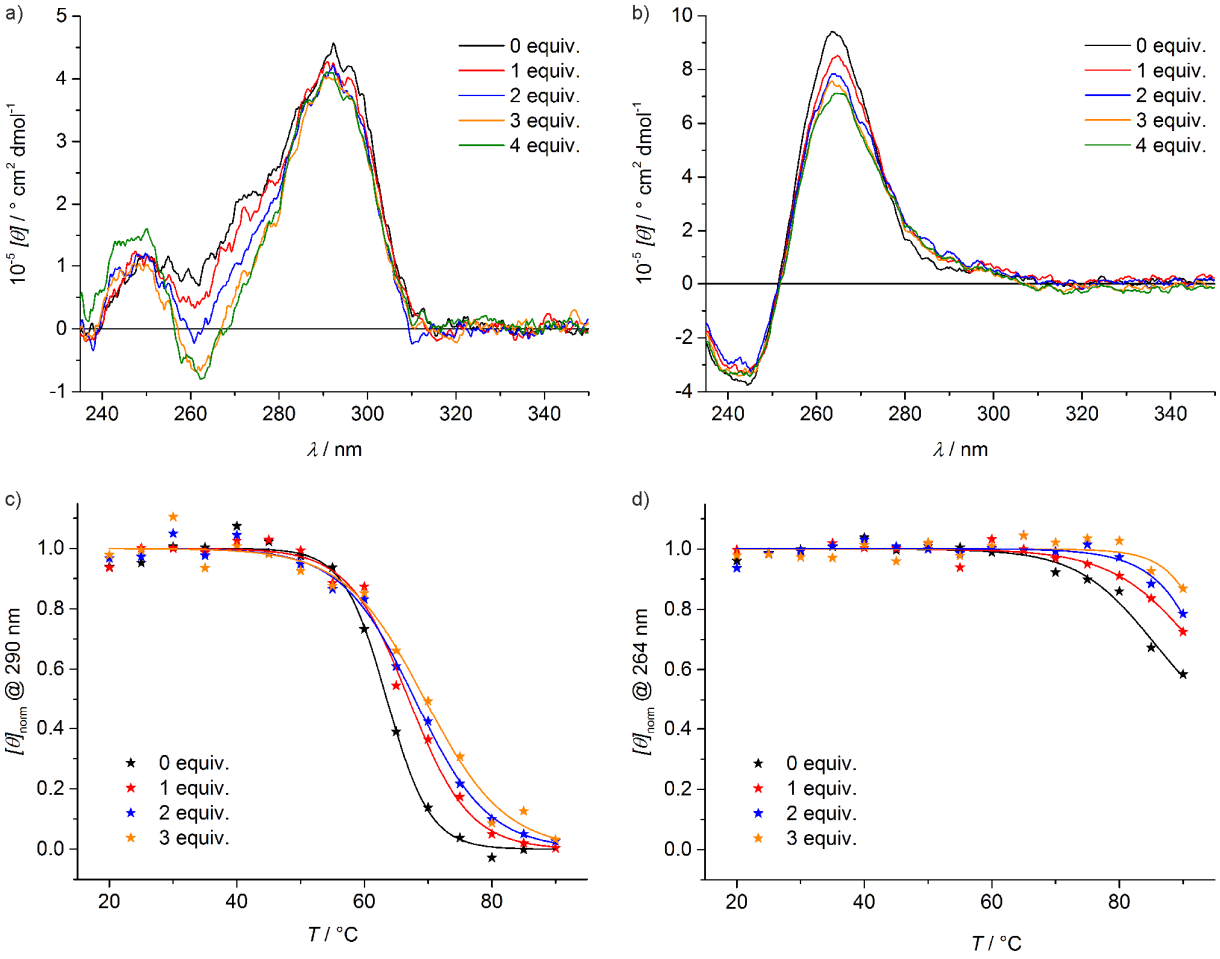

Fig. S1. CD spectra of a) H-telo and b) *c-myc* as well as melting curves of c) H-telo and d) *c-myc* in the presence of increasing amounts of [Pd(**1p**)Cl]Cl. Experimental details for the CD spectra: 1 μM oligonucleotide, 60 mM KCl, 5 mM MOPS (pH 7.4), 0 → 4 μM [Pd(**1p**)Cl]Cl, 20 °C, 1 cm optical path length; experimental details for the melting curves: 1 μM oligonucleotide, 60 mM KCl, 5 mM MOPS (pH 7.4), 0 → 3 μM [Pd(**1p**)Cl]Cl, 1 cm optical path length.

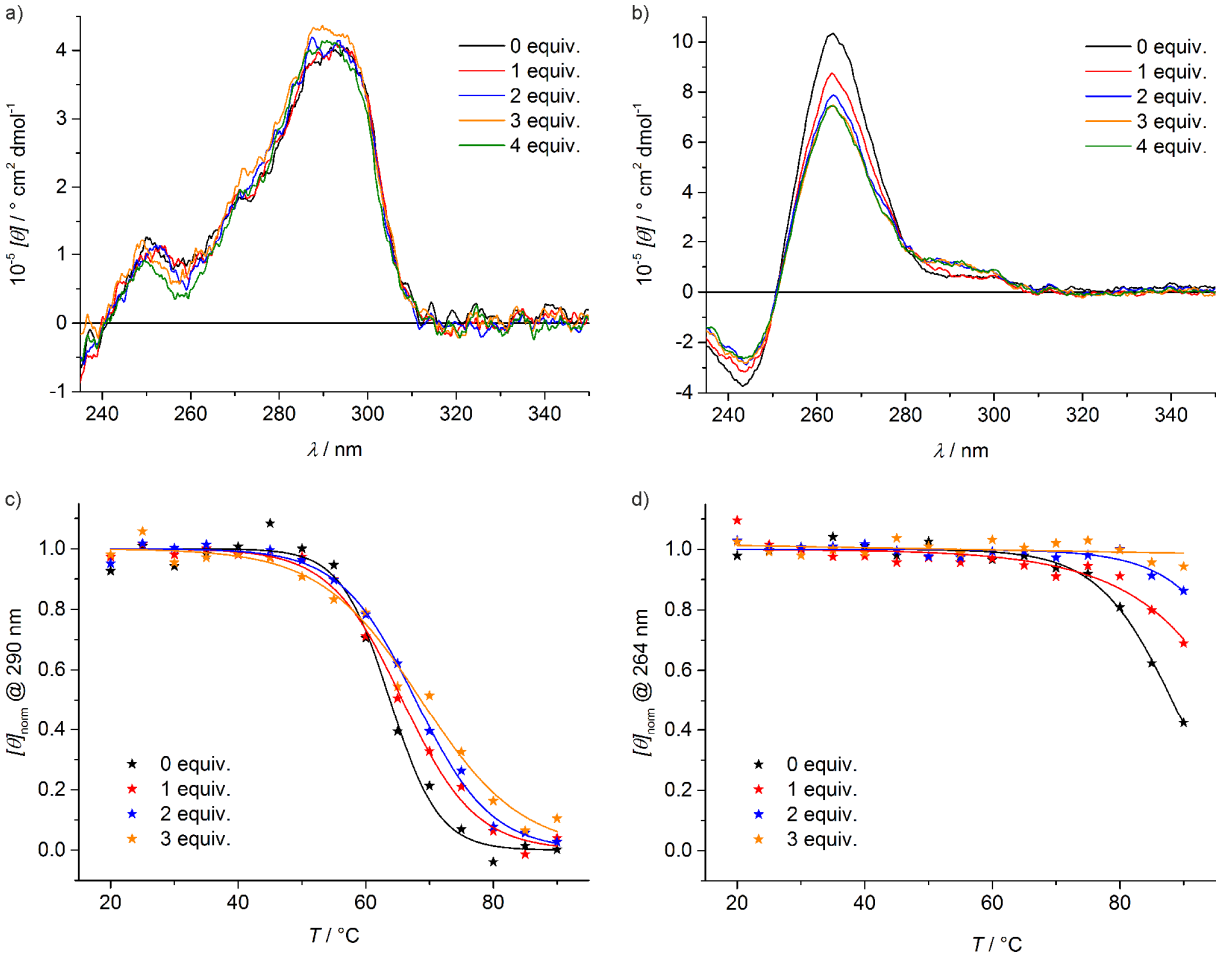

Fig. S2. CD spectra of a) H-telo and b) *c-myc* as well as melting curves of c) H-telo and d) *c-myc* in the presence of increasing amounts of [Pt(**1p**)Cl]Cl. Experimental details for the CD spectra: 1 μM oligonucleotide, 60 mM KCl, 5 mM MOPS (pH 7.4), 0 → 4 μM [Pt(**1p**)Cl]Cl, 20 °C, 1 cm optical path length; experimental details for the melting curves: 1 μM oligonucleotide, 60 mM KCl, 5 mM MOPS (pH 7.4), 0 → 3 μM [Pt(**1p**)Cl]Cl, 1 cm optical path length.

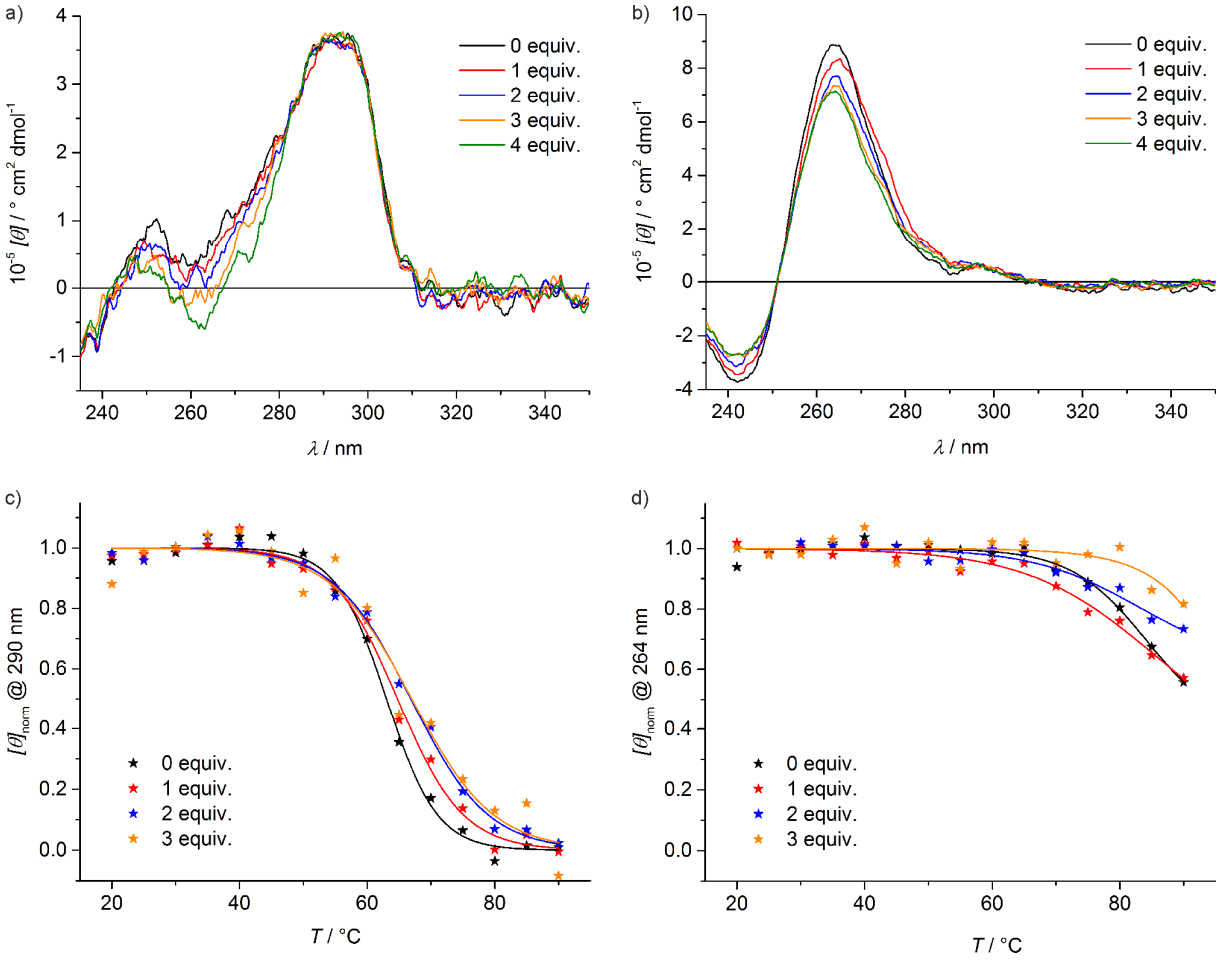

Fig. S3. CD spectra of a) H-telo and b) *c-myc* as well as melting curves of c) H-telo and d) *c-myc* in the presence of increasing amounts of [Pd(**1q**)Cl]Cl. Experimental details for the CD spectra: 1 μM oligonucleotide, 60 mM KCl, 5 mM MOPS (pH 7.4), 0 → 4 μM [Pd(**1q**)Cl]Cl, 20 °C, 1 cm optical path length; experimental details for the melting curves: 1 μM oligonucleotide, 60 mM KCl, 5 mM MOPS (pH 7.4), 0 → 3 μM [Pd(**1q**)Cl]Cl, 1 cm optical path length.

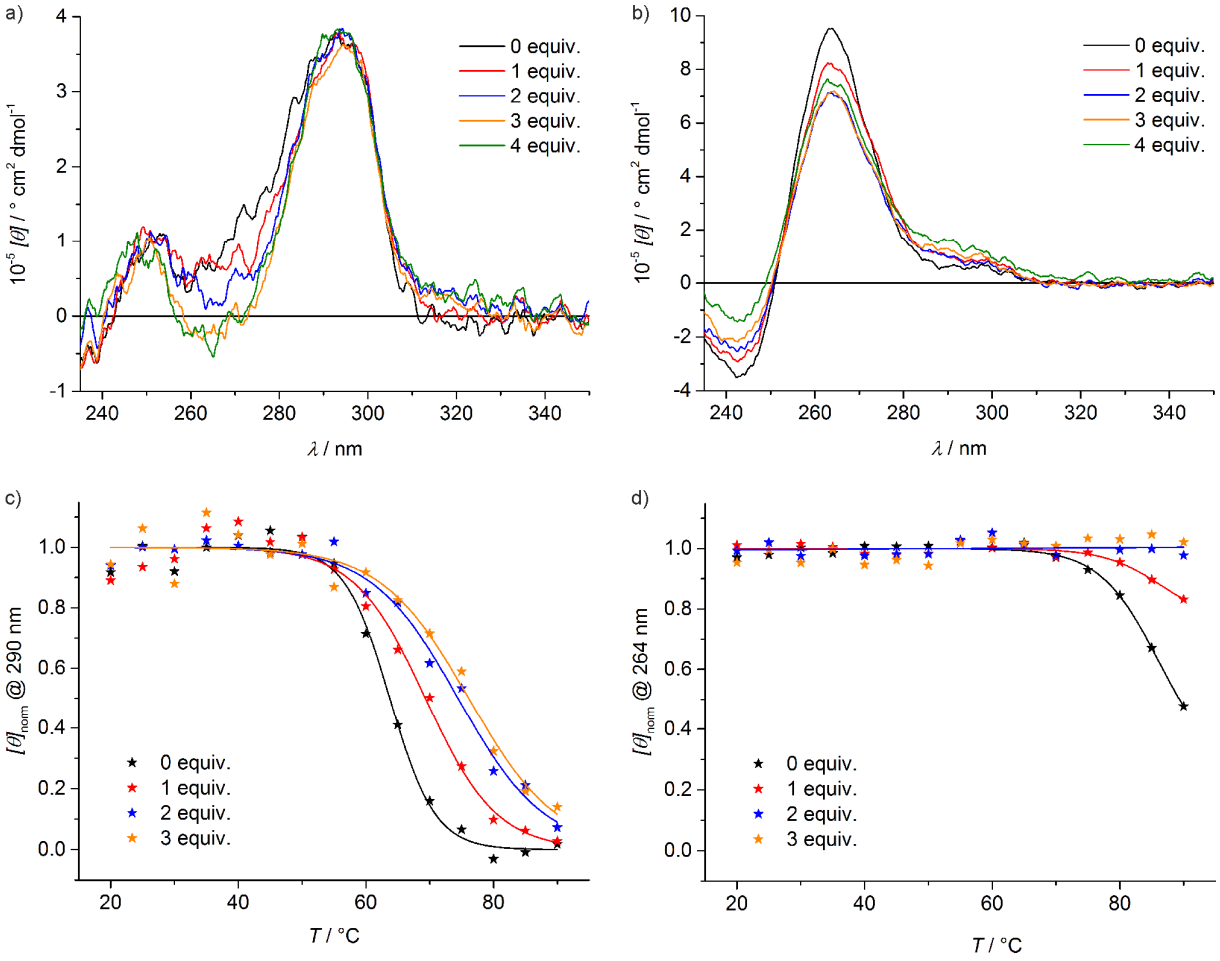

Fig. S4. CD spectra of a) H-telo and b) *c-myc* as well as melting curves of c) H-telo and d) *c-myc* in the presence of increasing amounts of [Pt(**1q**)Cl]Cl. Parts a) and b) of this figure are identical to Figure 4 in the main text. Experimental details for the CD spectra: 1 μM oligonucleotide, 60 mM KCl, 5 mM MOPS (pH 7.4), 0 → 4 μM [Pt(**1q**)Cl]Cl, 20 °C, 1 cm optical path length; experimental details for the melting curves: 1 μM oligonucleotide, 60 mM KCl, 5 mM MOPS (pH 7.4), 0 → 3 μM [Pt(**1q**)Cl]Cl, 1 cm optical path length.

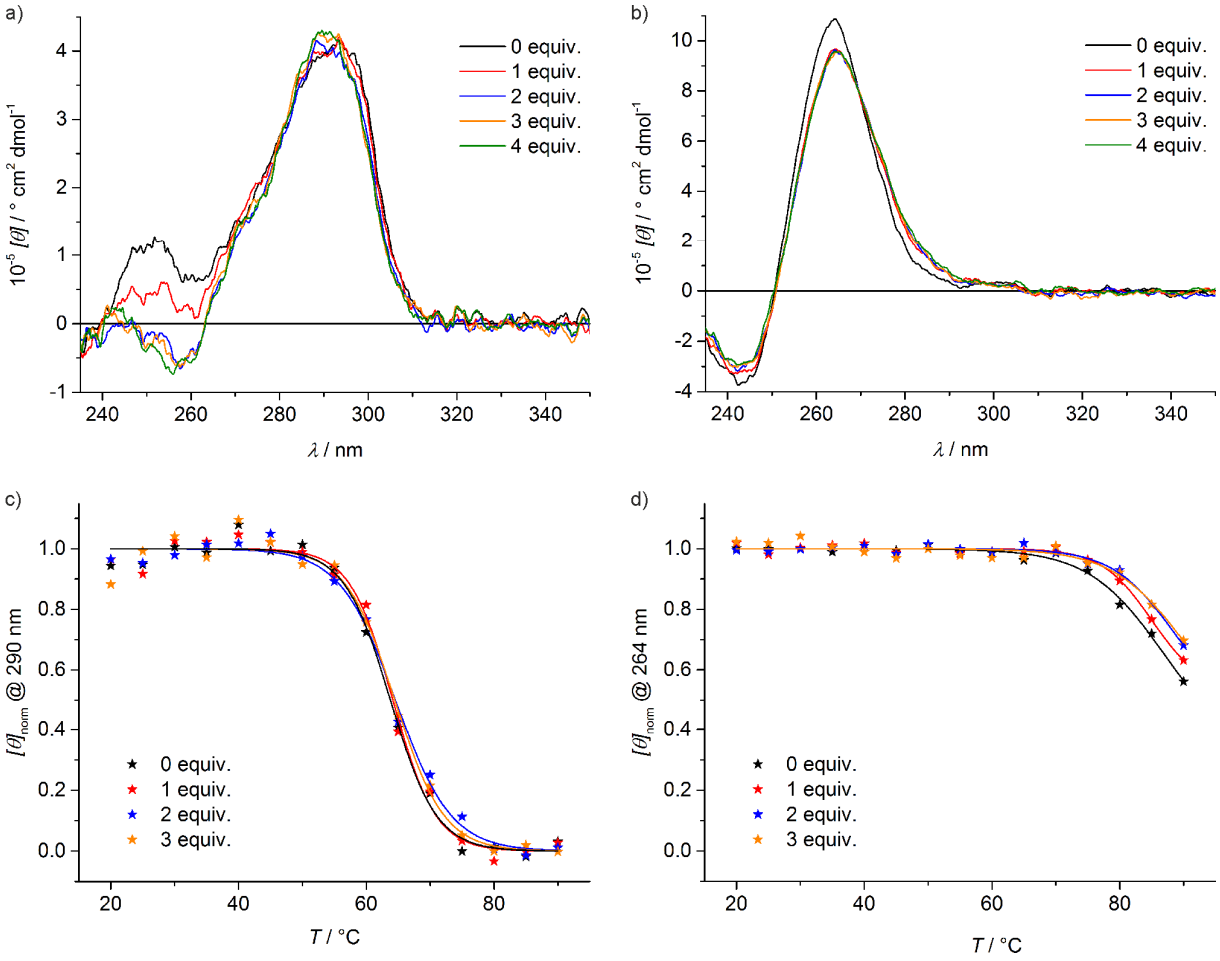

Fig. S5. CD spectra of a) H-telo and b) *c-myc* as well as melting curves of c) H-telo and d) *c-myc* in the presence of increasing amounts of [Pd(**2p**)Cl]. Experimental details for the CD spectra: 1 μM oligonucleotide, 60 mM KCl, 5 mM MOPS (pH 7.4), 0 → 4 μM [Pd(**2p**)Cl], 20 °C, 1 cm optical path length; experimental details for the melting curves: 1 μM oligonucleotide, 60 mM KCl, 5 mM MOPS (pH 7.4), 0 → 3 μM [Pd(**2p**)Cl], 1 cm optical path length.

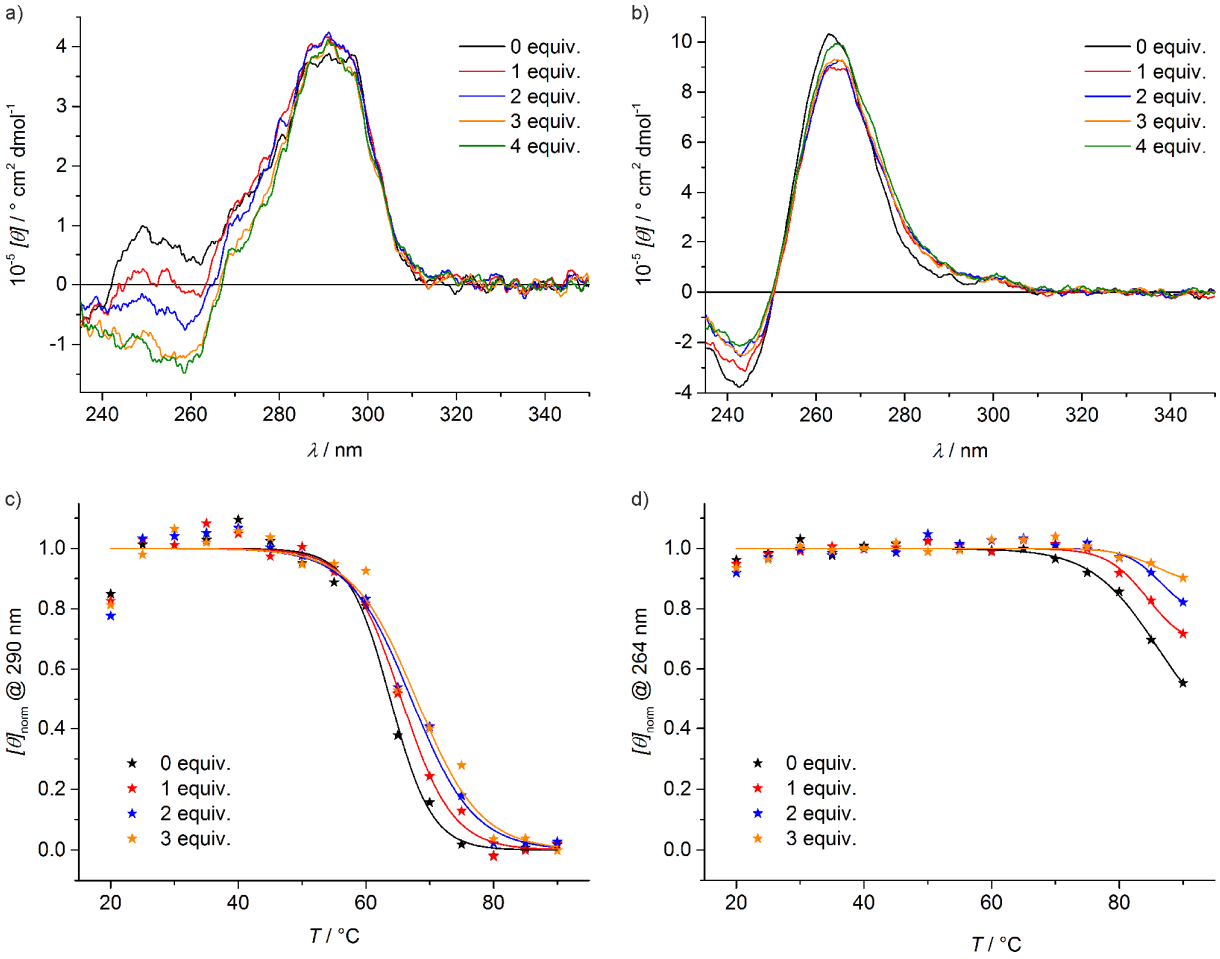

Fig. S6. CD spectra of a) H-telo and b) *c-myc* as well as melting curves of c) H-telo and d) *c-myc* in the presence of increasing amounts of [Pd(**2q**)Cl]. The data presented in parts a) and b) are identical to those shown in Fig. 5 in the main text. Experimental details for the CD spectra: 1 μM oligonucleotide, 60 mM KCl, 5 mM MOPS (pH 7.4), 0 → 4 μM [Pd(**2q**)Cl], 20 °C, 1 cm optical path length; experimental details for the melting curves: 1 μM oligonucleotide, 60 mM KCl, 5 mM MOPS (pH 7.4), 0 → 3 μM [Pd(**2q**)Cl], 1 cm optical path length.

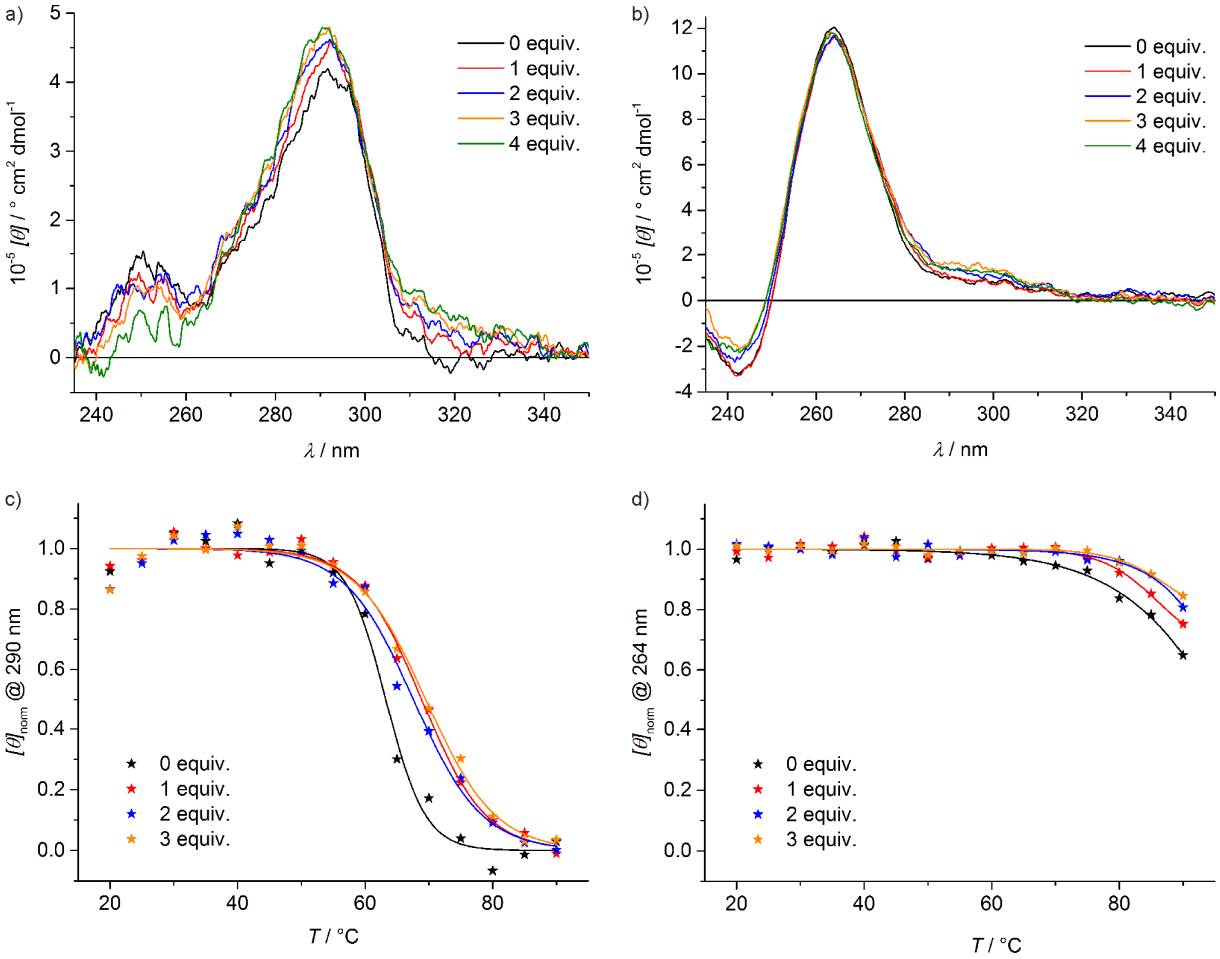

Fig. S7. CD spectra of a) H-telo and b) *c-myc* as well as melting curves of c) H-telo and d) *c-myc* in the presence of increasing amounts of [Pd(**3q**)Cl]. Experimental details for the CD spectra: 1 µM oligonucleotide, 60 mM KCl, 5 mM MOPS (pH 7.4), 0 → 4 µM [Pd(**3q**)Cl], 20 °C, 1 cm optical path length; experimental details for the melting curves: 1 µM oligonucleotide, 60 mM KCl, 5 mM MOPS (pH 7.4), 0 → 3 µM [Pd(**3q**)Cl], 1 cm optical path length.

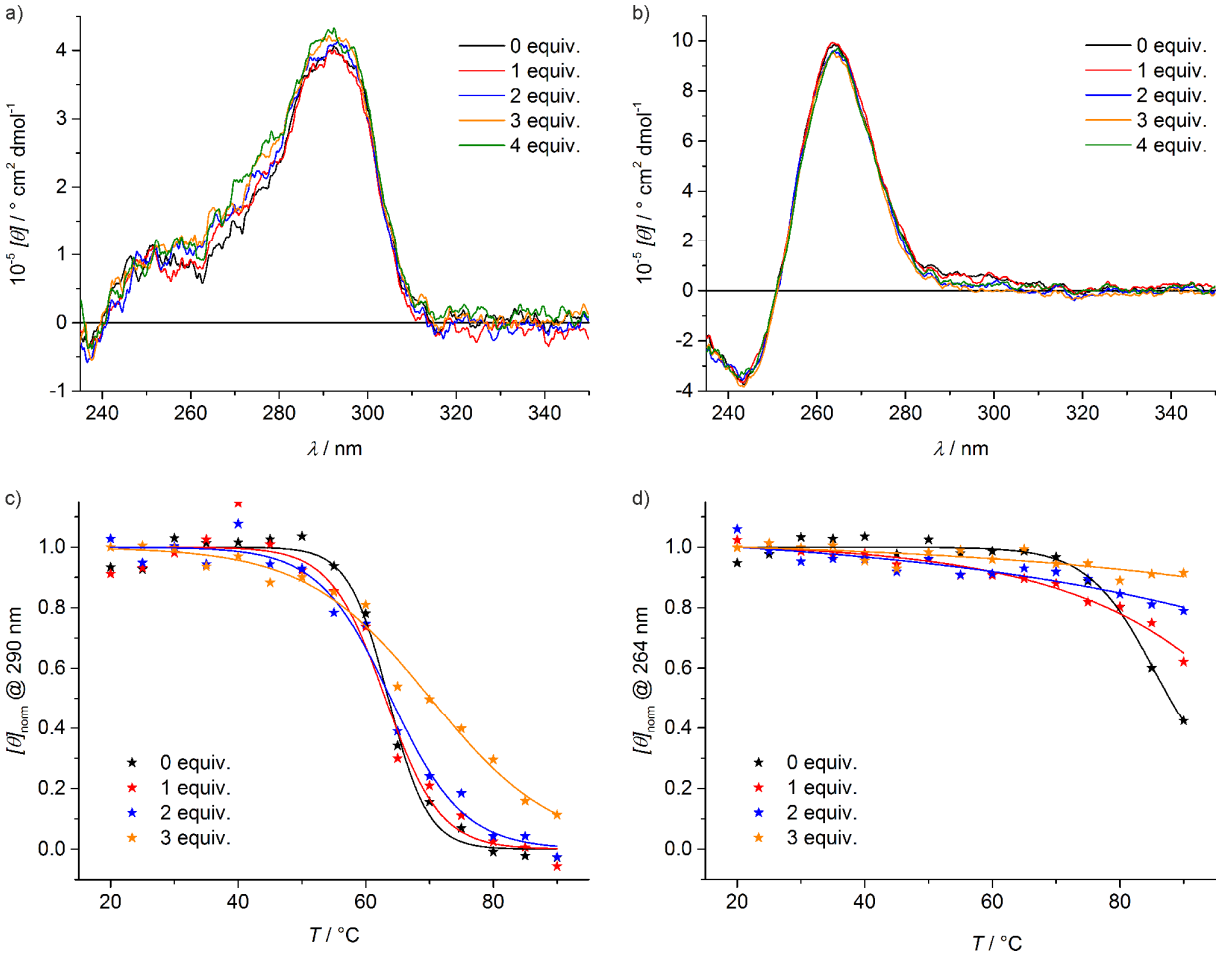

Fig. S8. CD spectra of a) H-telo and b) *c-myc* as well as melting curves of c) H-telo and d) *c-myc* in the presence of increasing amounts of [Pt(**3q**)Cl]. Experimental details for the CD spectra: 1 μM oligonucleotide, 60 mM KCl, 5 mM MOPS (pH 7.4), 0 → 4 μM [Pt(**3q**)Cl], 20 °C, 1 cm optical path length; experimental details for the melting curves: 1 μM oligonucleotide, 60 mM KCl, 5 mM MOPS (pH 7.4), 0 → 3 μM [Pt(**3q**)Cl], 1 cm optical path length.

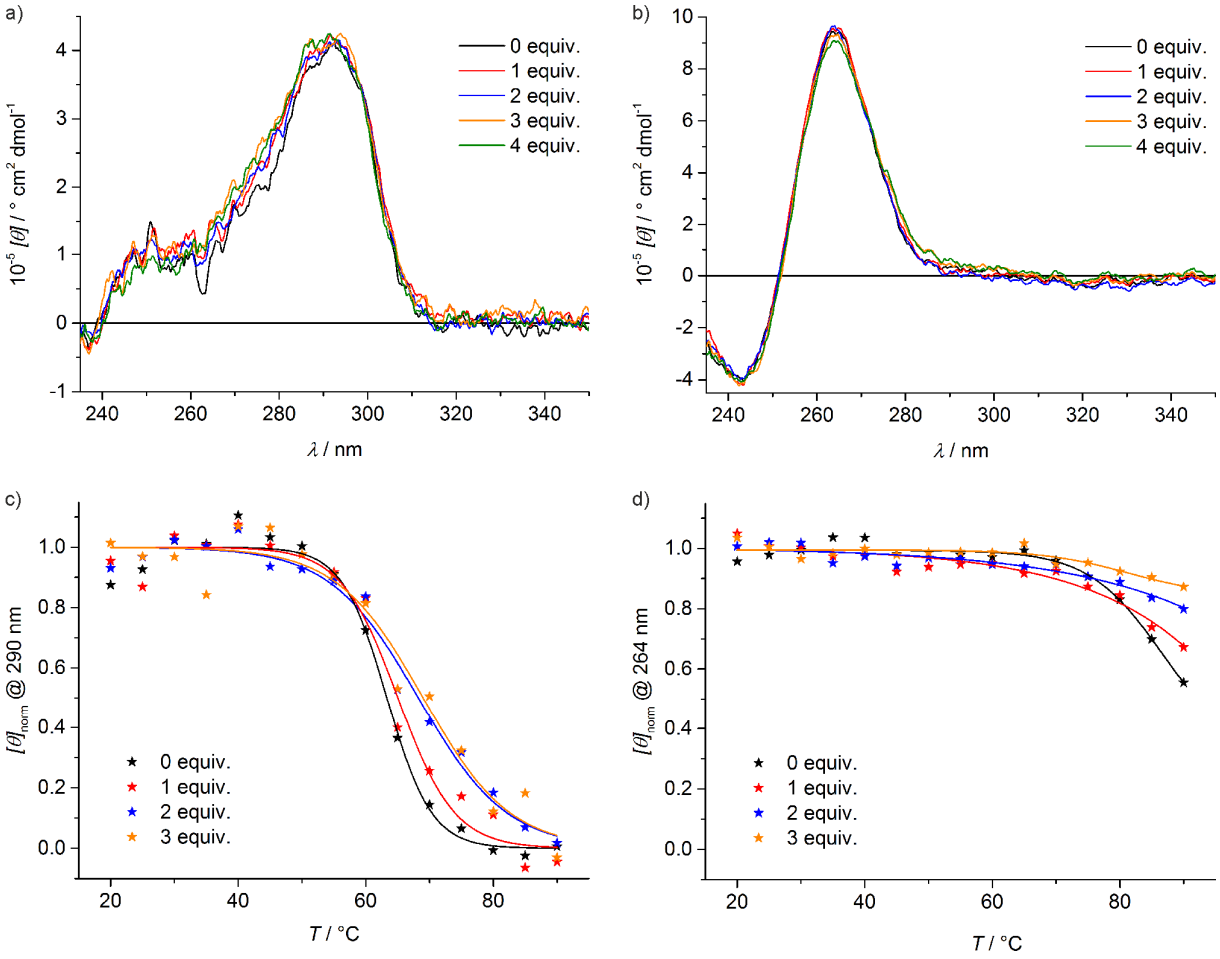

Fig. S9. CD spectra of a) H-telo and b) *c-myc* as well as melting curves of c) H-telo and d) *c-myc* in the presence of increasing amounts of [Pt(**4q**)Cl]. Experimental details for the CD spectra: 1 µM oligonucleotide, 60 mM KCl, 5 mM MOPS (pH 7.4), 0 → 4 µM [Pt(**4q**)Cl], 20 °C, 1 cm optical path length; experimental details for the melting curves: 1 µM oligonucleotide, 60 mM KCl, 5 mM MOPS (pH 7.4), 0 → 3 µM [Pd(**4q**)Cl], 1 cm optical path length.

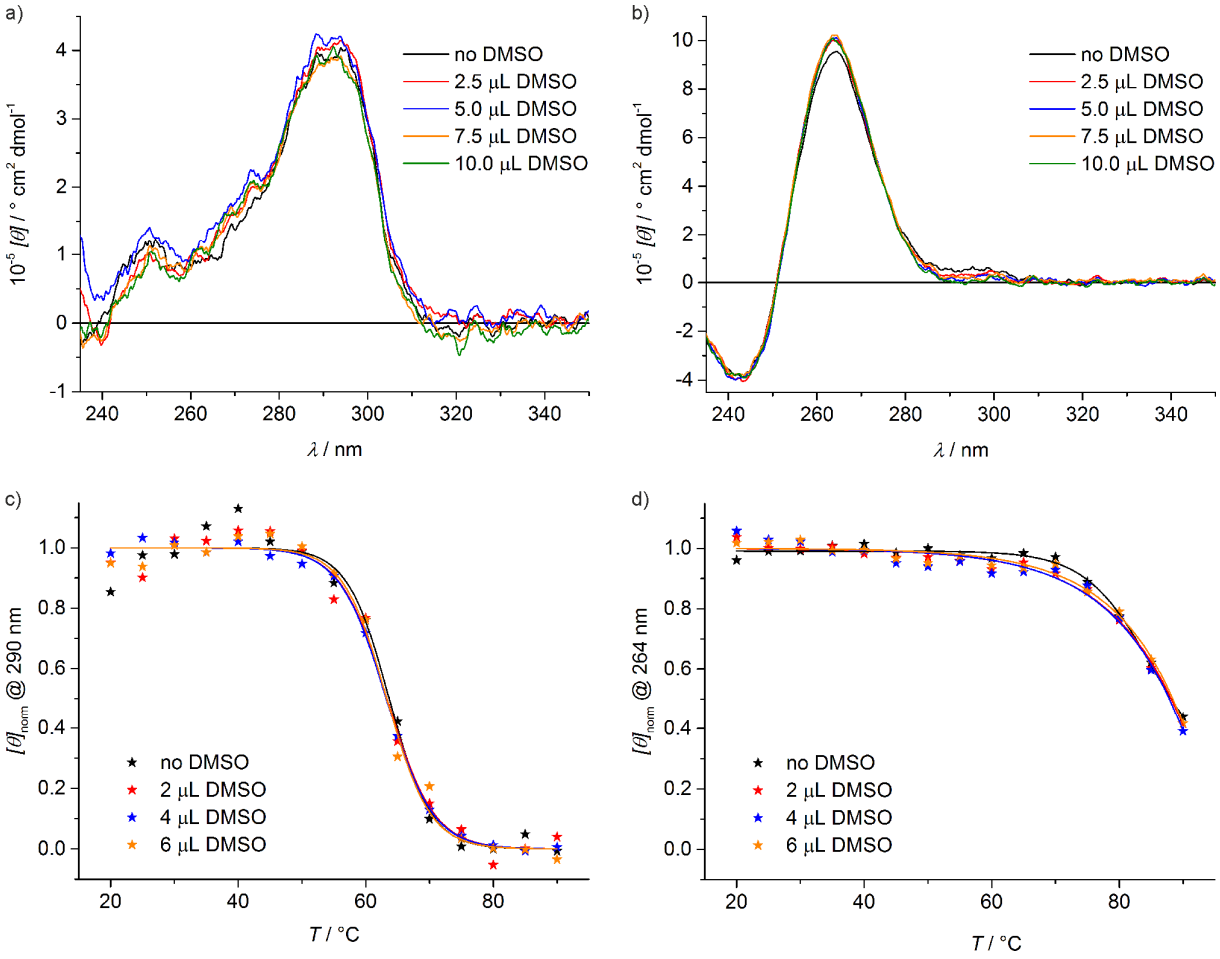

Fig. S10. CD spectra of a) H-telo and b) *c-myc* as well as melting curves of c) H-telo and d) *c-myc* in the presence of increasing amounts of DMSO. The volume of DMSO used in these titrations is identical to the one used in the respective titrations with the metal complexes. Obviously, the CD spectrum of H-telo does not change significantly upon the addition of DMSO. Hence, no correction was applied in the titrations with the neutral complexes. In contrast, the addition of 2.5 µL of DMSO to *c-myc* leads to a slight change in the Cotton effect at 264 nm. To account for this effect, 3.0 µL of DMSO were added to the *c-myc* solutions prior to all titrations with a neutral metal complex. Experimental details for the CD spectra: 1 µM oligonucleotide, 60 mM KCl, 5 mM MOPS (pH 7.4), 0 → 10 µL DMSO, 20 °C, 1 cm optical path length; experimental details for the melting curves: 1 µM oligonucleotide, 60 mM KCl, 5 mM MOPS (pH 7.4), 0 → 6 µL DMSO, 1 cm optical path length.

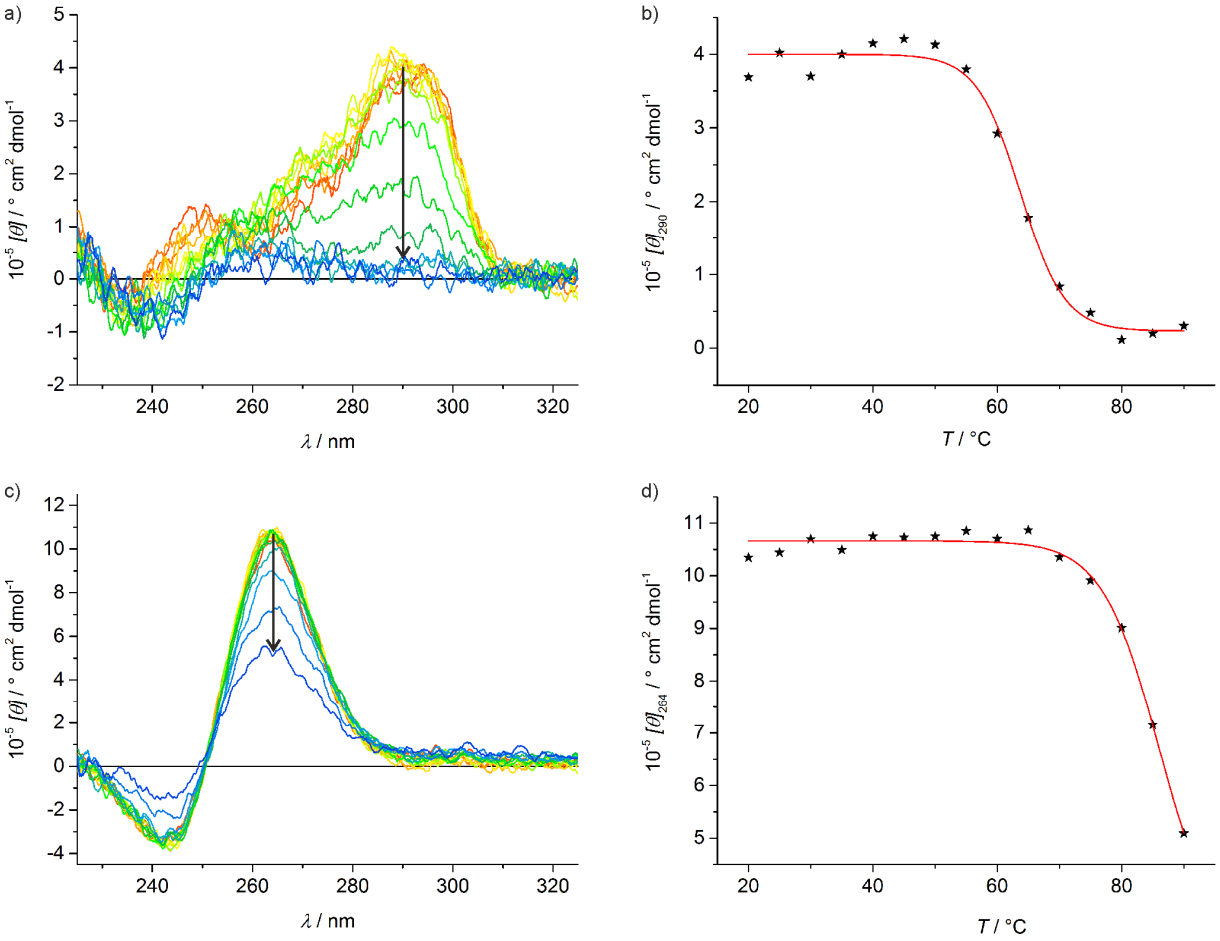

Fig. S11. Temperature-dependent CD spectra of a) H-telo and c) *c-myc*, recorded in the temperature range from 20 to 90 °C in steps of 5 °C. The melting of the quadruplexes can be followed at wavelengths of b) 290 nm for H-telo and d) 264 nm for *c-myc*. Experimental conditions: 1 μM quadruplex, 60 mM KCl, 5 mM MOPS (pH 7.4), 1 cm optical path length. Because of the incomplete melting of *c-myc* even at 90 °C, the experiments were repeated at reduced KCl concentrations (1 mM rather than 60 mM). Even at such low KCl concentrations, the melting temperature did not decrease. For better comparison, only the data for 60 mM KCl are used and discussed in the text.

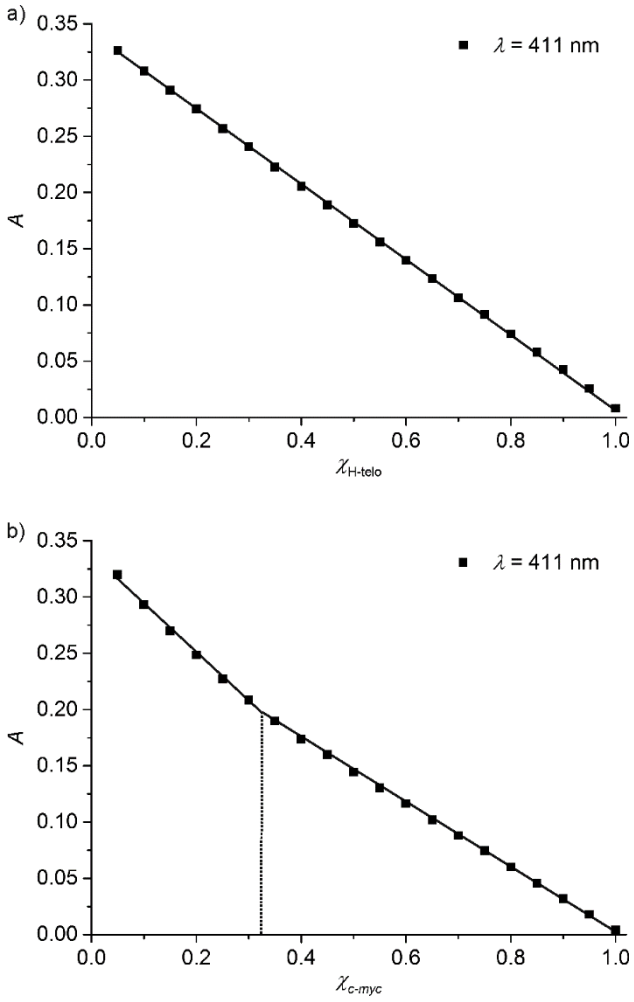

Fig. S12. Job plots for the binding of [Pd(**1p**)Cl]Cl to a) H-telo and b) *c-myc*. Experimental details of the UV/Vis spectra used to generate the Job plots: 45 μM combined concentration of quadruplex and [Pd(**1p**)Cl]Cl, 60 mM KCl, 5 mM MOPS (pH 7.4), 20 °C, 1 cm optical path length.

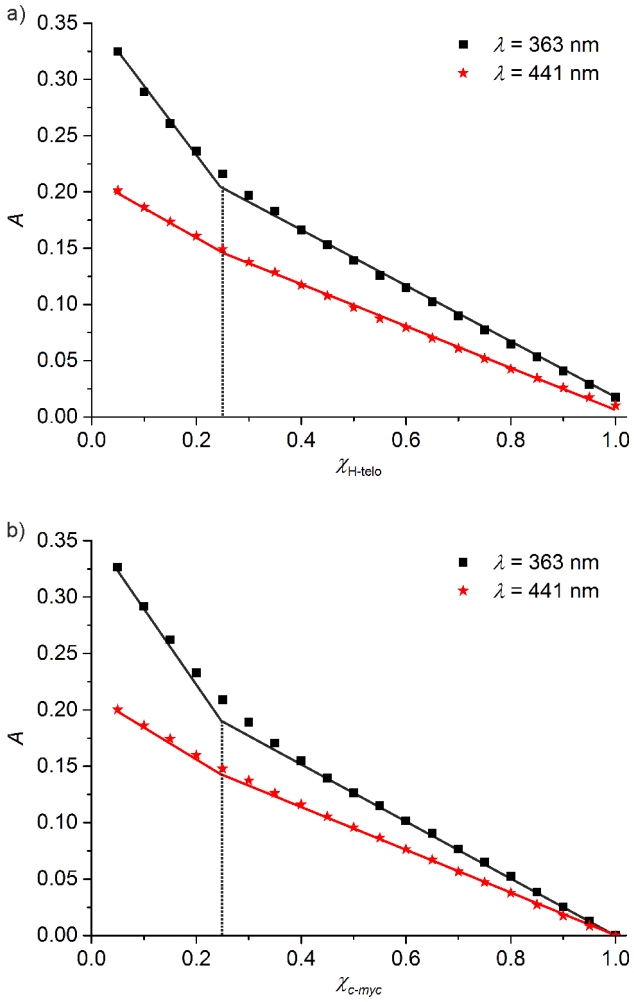

Fig. S13. Job plots for the binding of [Pt(**1p**)Cl]Cl to a) H-telo and b) *c-myc*. Experimental details of the UV/Vis spectra used to generate the Job plots: 45 μM combined concentration of quadruplex and [Pt(**1p**)Cl]Cl, 60 mM KCl, 5 mM MOPS (pH 7.4), 20 °C, 1 cm optical path length.

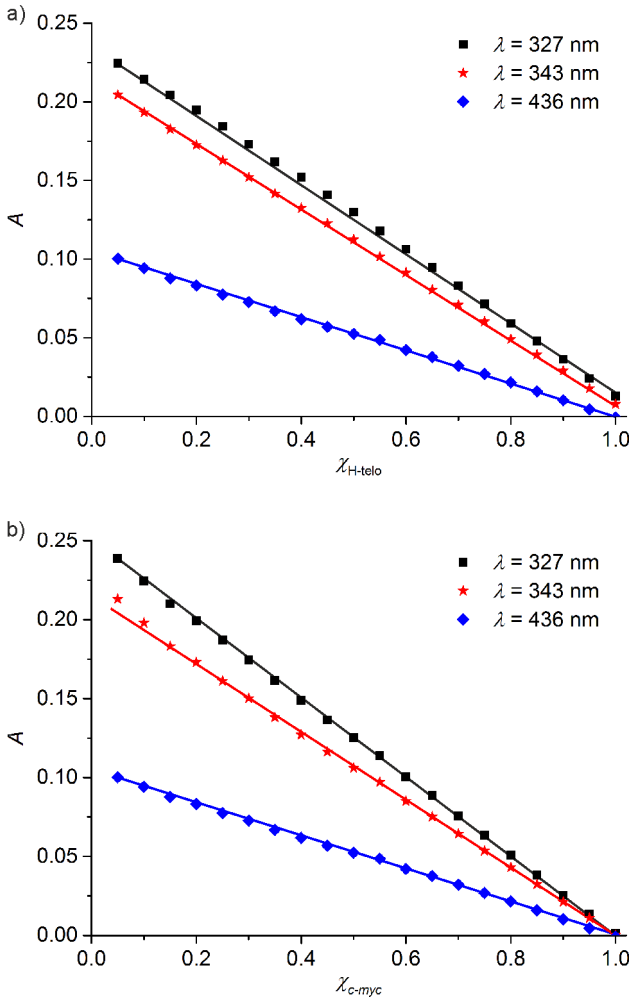

Fig. S14. Job plots for the binding of [Pd(**1q**)Cl]Cl to a) H-telo and b) *c-myc*. Experimental details of the UV/Vis spectra used to generate the Job plots: 45 μM combined concentration of quadruplex and [Pd(**1q**)Cl]Cl, 60 mM KCl, 5 mM MOPS (pH 7.4), 20 °C, 1 cm optical path length.

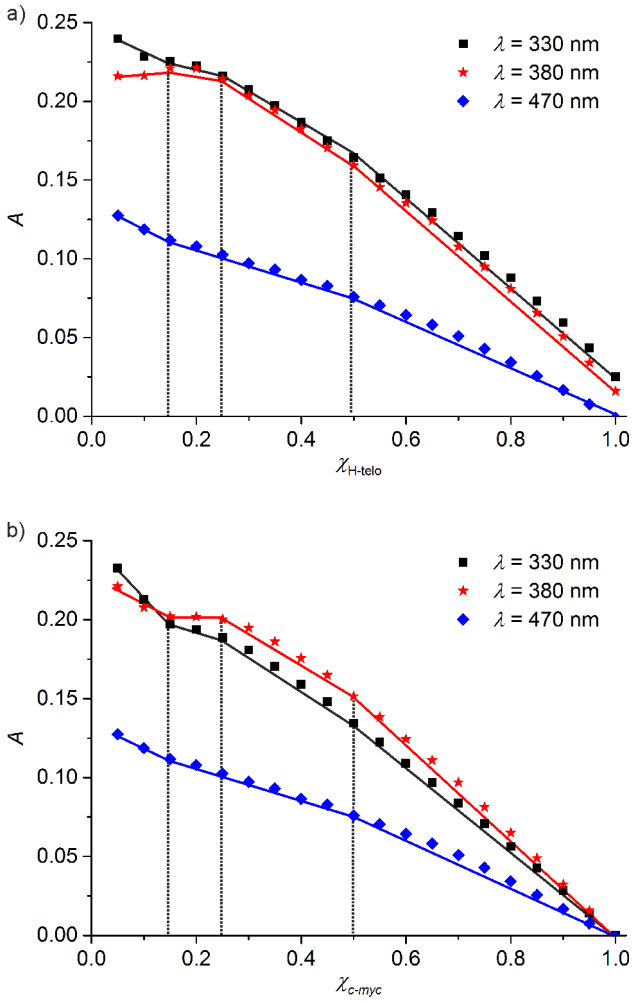

Fig. S15. Job plots for the binding of [Pt(**1q**)Cl]Cl to a) H-telo and b) *c-myc*. Experimental details of the UV/Vis spectra used to generate the Job plots: 45 μM combined concentration of quadruplex and [Pt(**1q**)Cl]Cl, 60 mM KCl, 5 mM MOPS (pH 7.4), 20 °C, 1 cm optical path length.

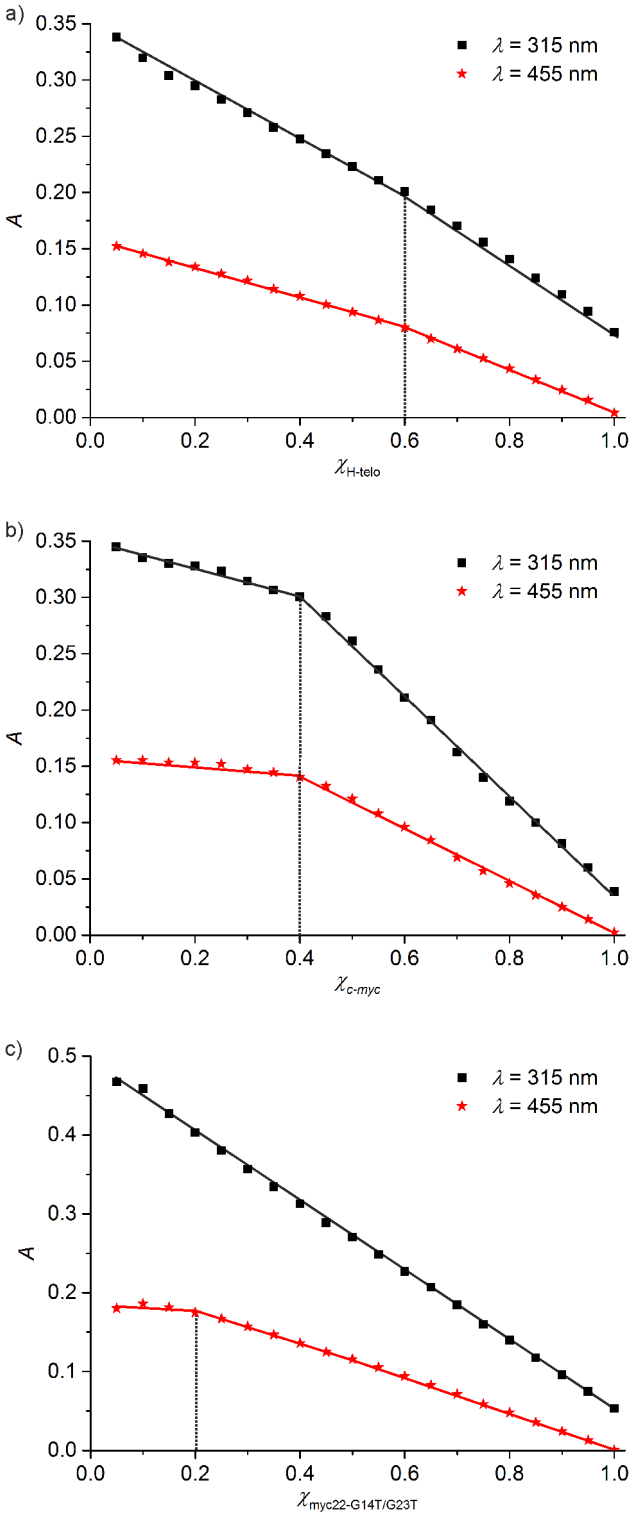

Fig. S16. Job plots for the binding of [Pd(**2p**)Cl] to a) H-telo, b) *c-myc* and c) myc22-G14T/G23T. Experimental details of the UV/Vis spectra used to generate the Job plots: 45 μM combined concentration of quadruplex and [Pd(**2p**)Cl], 60 mM KCl, 5 mM MOPS (pH 7.4), 5% DMSO, 20 °C, 1 cm optical path length.

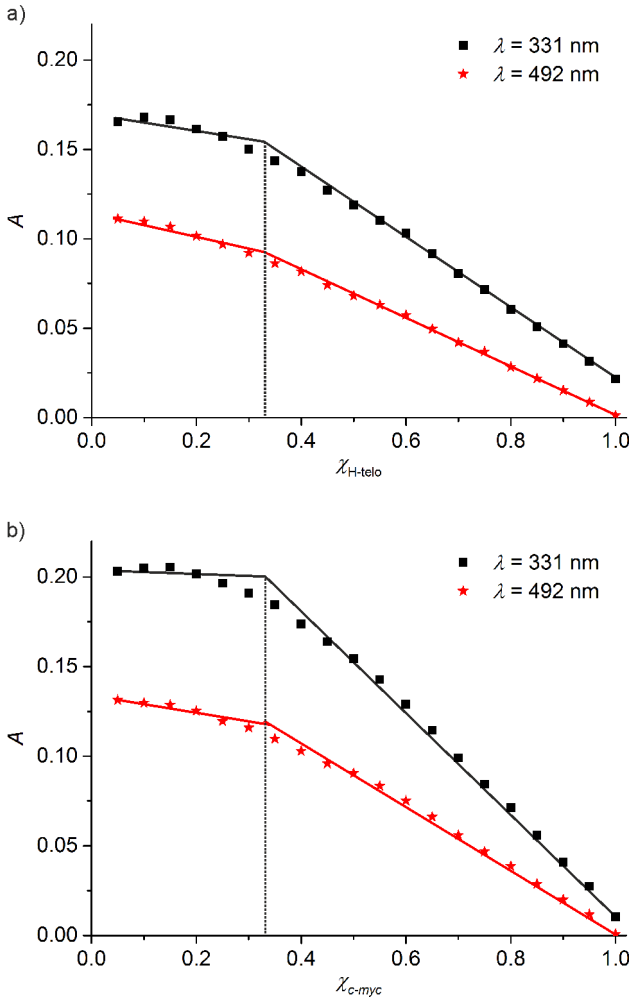

Fig. S17. Job plots for the binding of [Pd(**2q**)Cl] to a) H-telo and b) *c-myc*. Experimental details of the UV/Vis spectra used to generate the Job plots: 45 μM combined concentration of quadruplex and [Pd(**2q**)Cl], 60 mM KCl, 5 mM MOPS (pH 7.4), 5% DMSO, 20 °C, 1 cm optical path length.

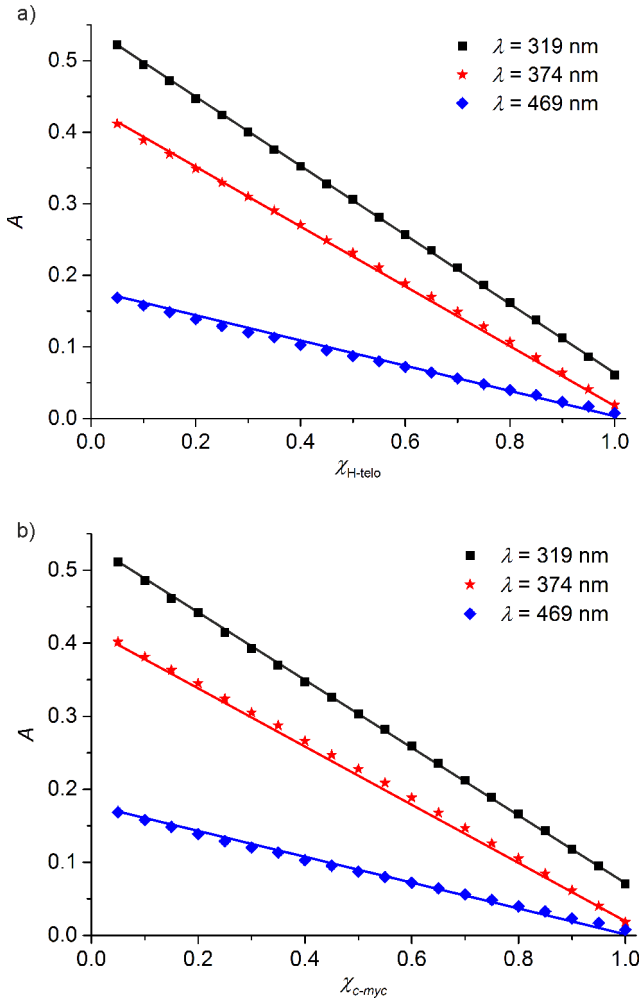

Fig. S18. Job plots for the binding of [Pd(**3q**)Cl] to a) H-telo and b) *c-myc*. Experimental details of the UV/Vis spectra used to generate the Job plots: 45 μM combined concentration of quadruplex and [Pd(**3q**)Cl], 60 mM KCl, 5 mM MOPS (pH 7.4), 5% DMSO, 20 °C, 1 cm optical path length.

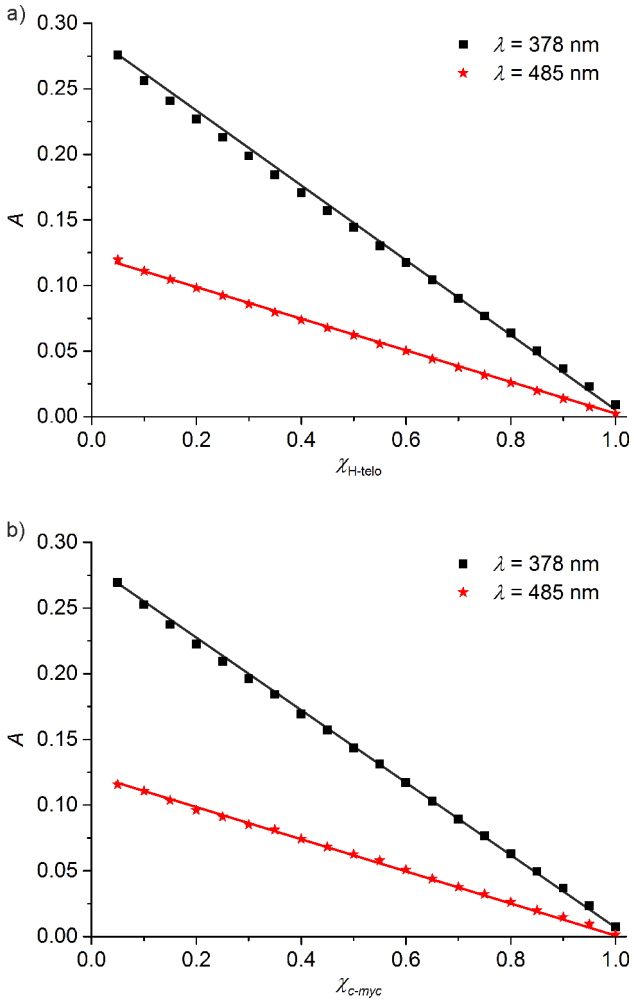

Fig. S19. Job plots for the binding of [Pt(**3q**)Cl] to a) H-telo and b) *c-myc*. Experimental details of the UV/Vis spectra used to generate the Job plots: 45 μM combined concentration of quadruplex and [Pt(**3q**)Cl], 60 mM KCl, 5 mM MOPS (pH 7.4), 5% DMSO, 20 °C, 1 cm optical path length.

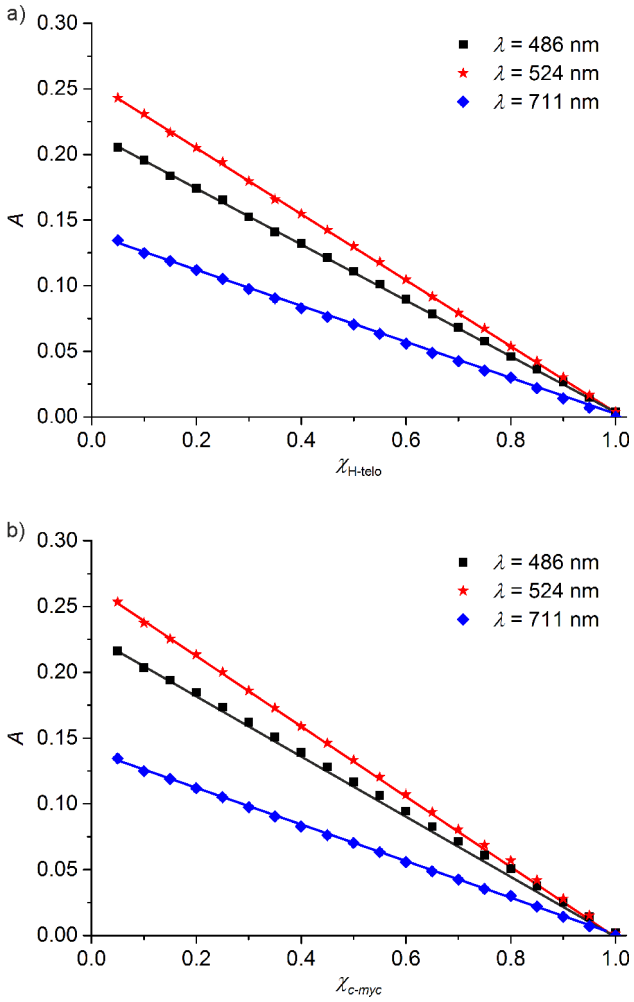

Fig. S20. Job plots for the binding of [Pt(**4q**)Cl] to a) H-telo and b) *c-myc*. Experimental details of the UV/Vis spectra used to generate the Job plots: 45 μM combined concentration of quadruplex and [Pt(**4q**)Cl], 60 mM KCl, 5 mM MOPS (pH 7.4), 5% DMSO, 20 °C, 1 cm optical path length.

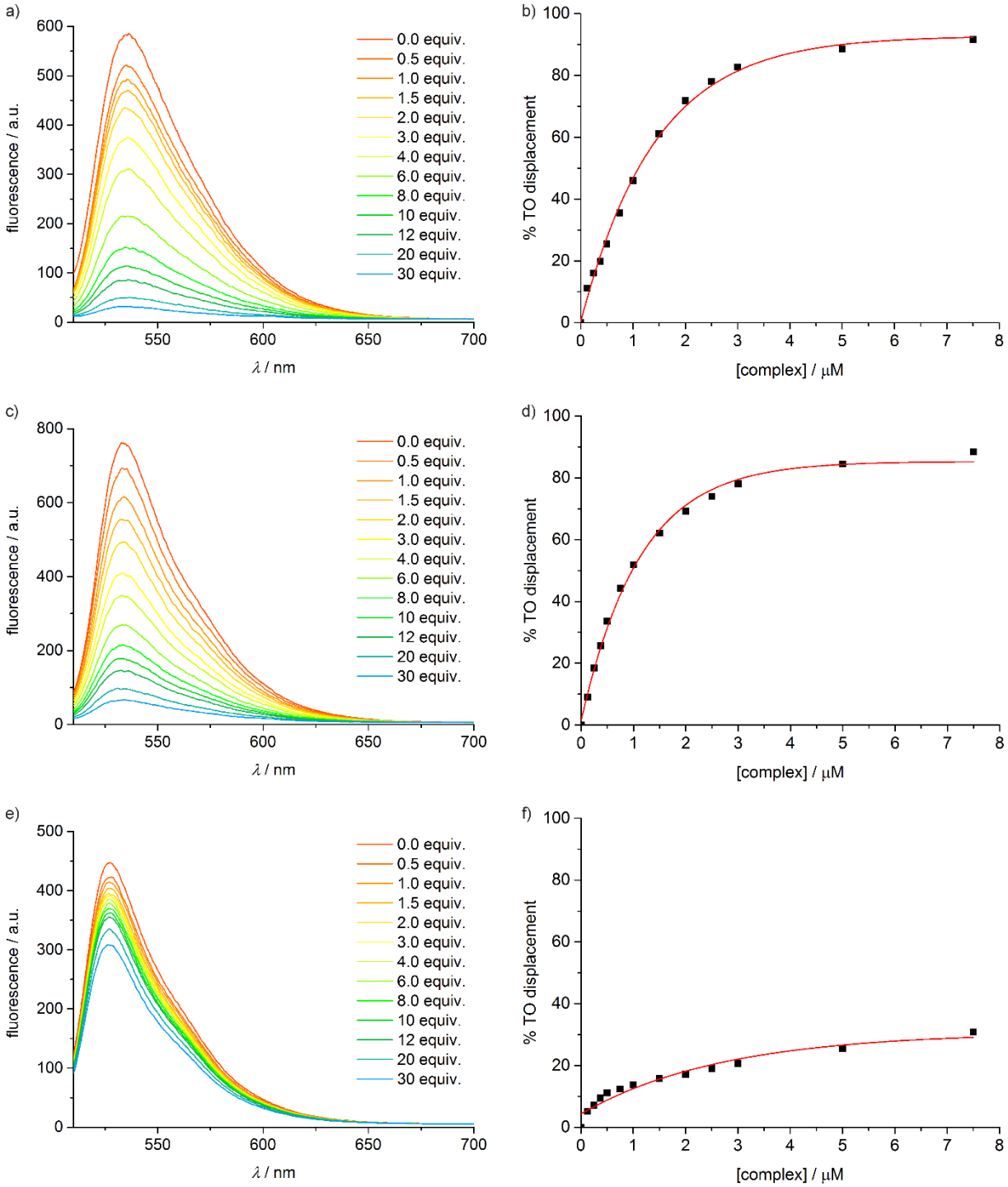

Fig. S21. Fluorescence spectra of TO intercalated into a) H-telo, c) *c-myc* and e) ds26 in the presence of increasing amounts of [Pd(**1p**)Cl]Cl as well as percentage TO displacement from b) H-telo, d) *c-myc* and f) ds26. Experimental details: 0.25 μM oligonucleotide, TO (0.5 μM for quadruplex DNA, 0.75 μM for ds26), 60 mM KCl, 5 mM MOPS (pH 7.4), 0 → 7.5 μM [Pd(**1p**)Cl]Cl, 1 cm optical path length.

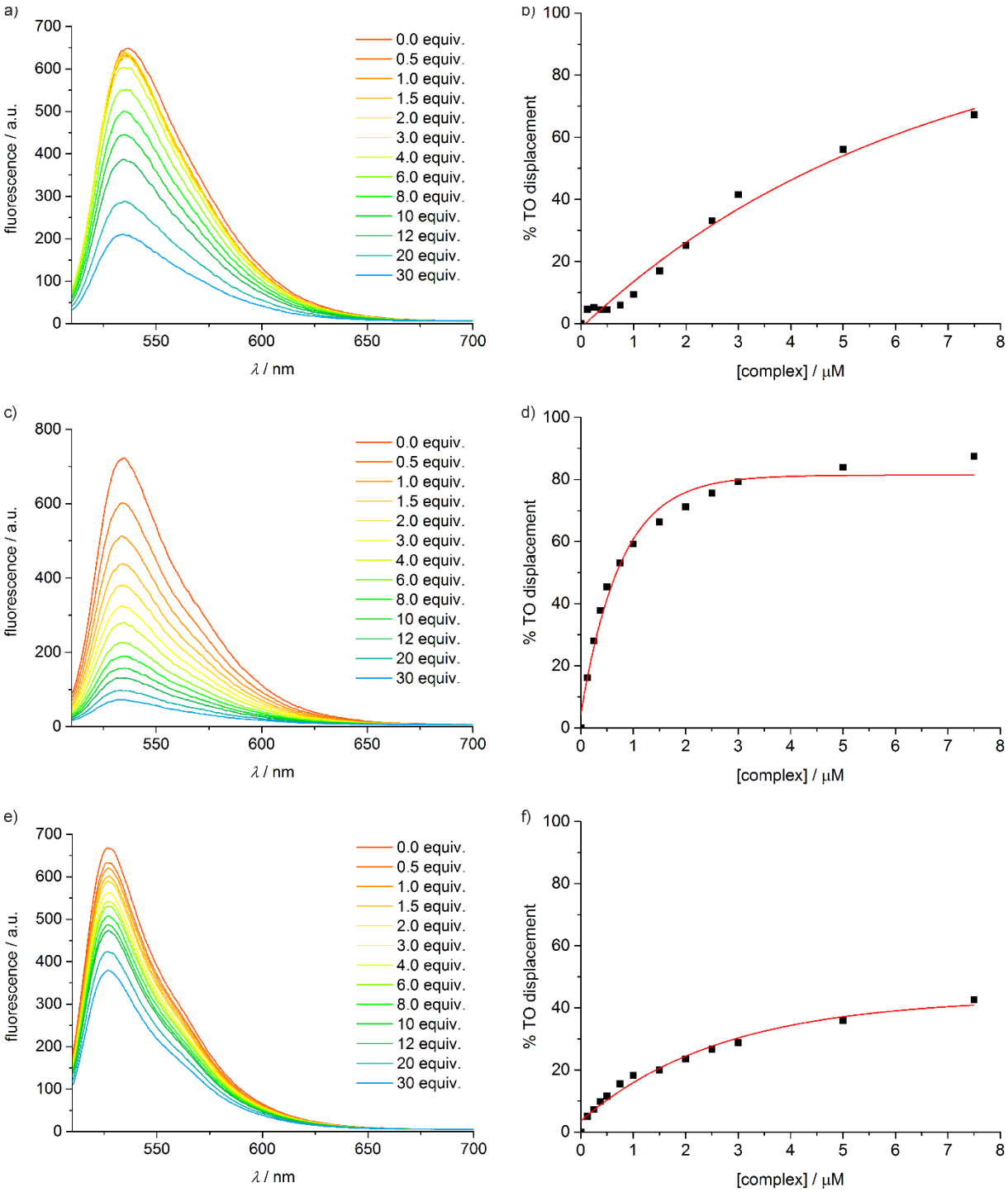

Fig. S22. Fluorescence spectra of TO intercalated into a) H-telo, c) *c-myc* and e) ds26 in the presence of increasing amounts of [Pt(**1p**)Cl]Cl as well as percentage TO displacement from b) H-telo, d) *c-myc* and f) ds26. Experimental details: 0.25 μM oligonucleotide, TO (0.5 μM for quadruplex DNA, 0.75 μM for ds26), 60 mM KCl, 5 mM MOPS (pH 7.4), 0 → 7.5 μM [Pt(**1p**)Cl]Cl, 1 cm optical path length.

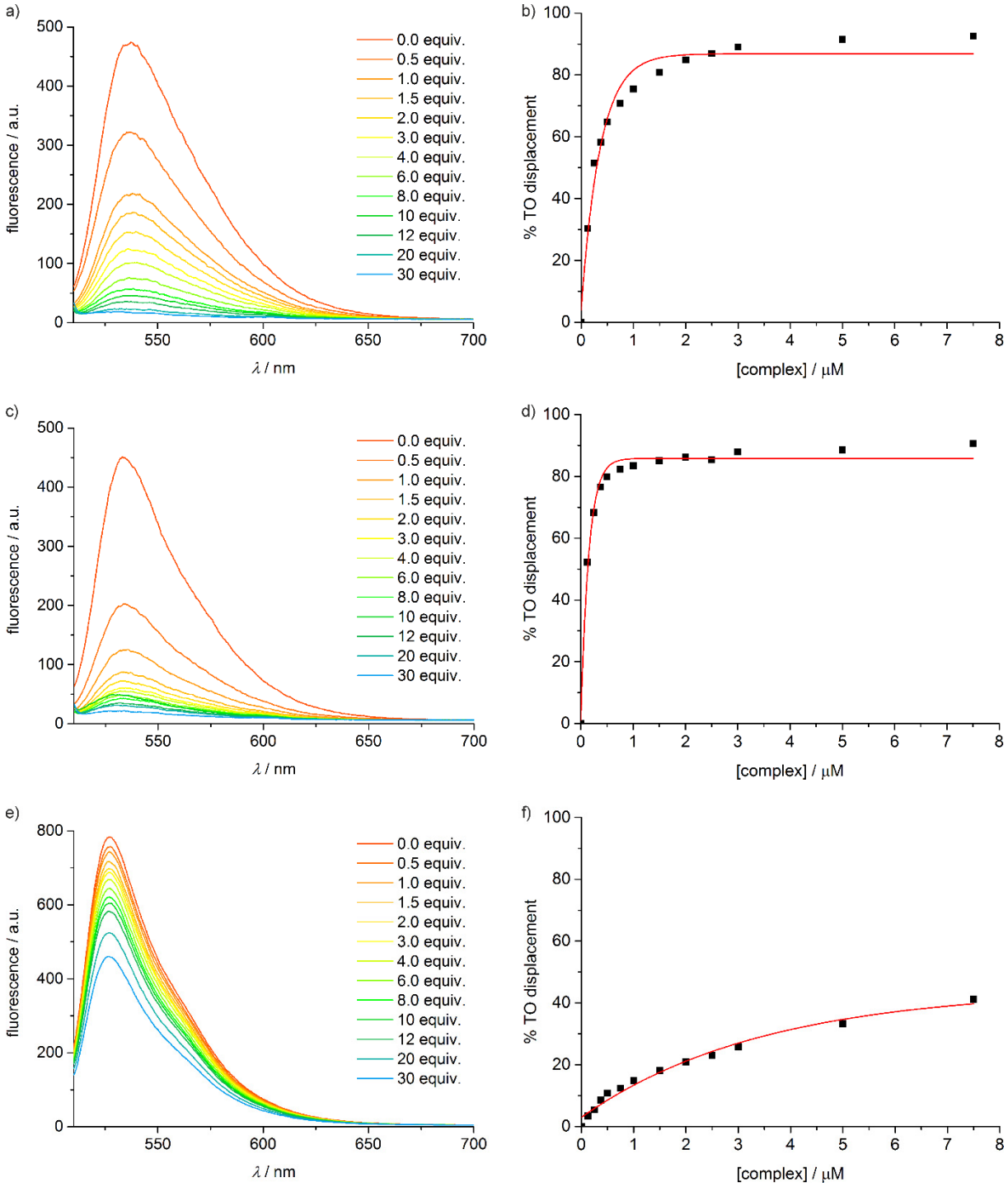

Fig. S23. Fluorescence spectra of TO intercalated into a) H-telo, c) *c-myc* and e) ds26 in the presence of increasing amounts of [Pd(**1q**)Cl]Cl as well as percentage TO displacement from b) H-telo, d) *c-myc* and f) ds26. Experimental details: 0.25 μM oligonucleotide, TO (0.5 μM for quadruplex DNA, 0.75 μM for ds26), 60 mM KCl, 5 mM MOPS (pH 7.4), 0 → 7.5 μM [Pd(**1q**)Cl]Cl, 1 cm optical path length.

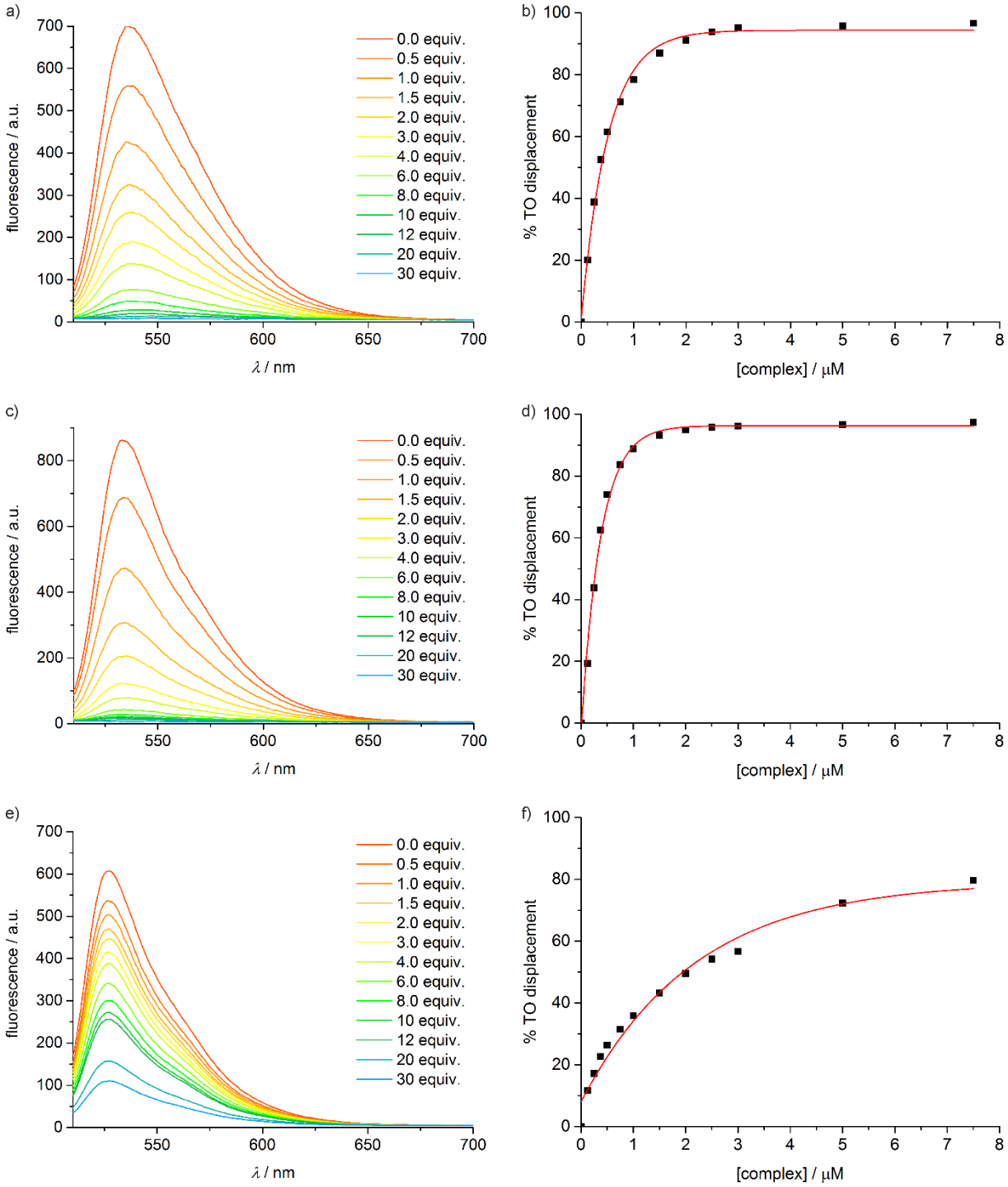

Fig. S24. Fluorescence spectra of TO intercalated into a) H-telo, c) *c-myc* and e) ds26 in the presence of increasing amounts of [Pt(**1q**)Cl]Cl as well as percentage TO displacement from b) H-telo, d) *c-myc* and f) ds26. Experimental details: 0.25 μM oligonucleotide, TO (0.5 μM for quadruplex DNA, 0.75 μM for ds26), 60 mM KCl, 5 mM MOPS (pH 7.4), 0 → 7.5 μM [Pt(**1q**)Cl]Cl, 1 cm optical path length.

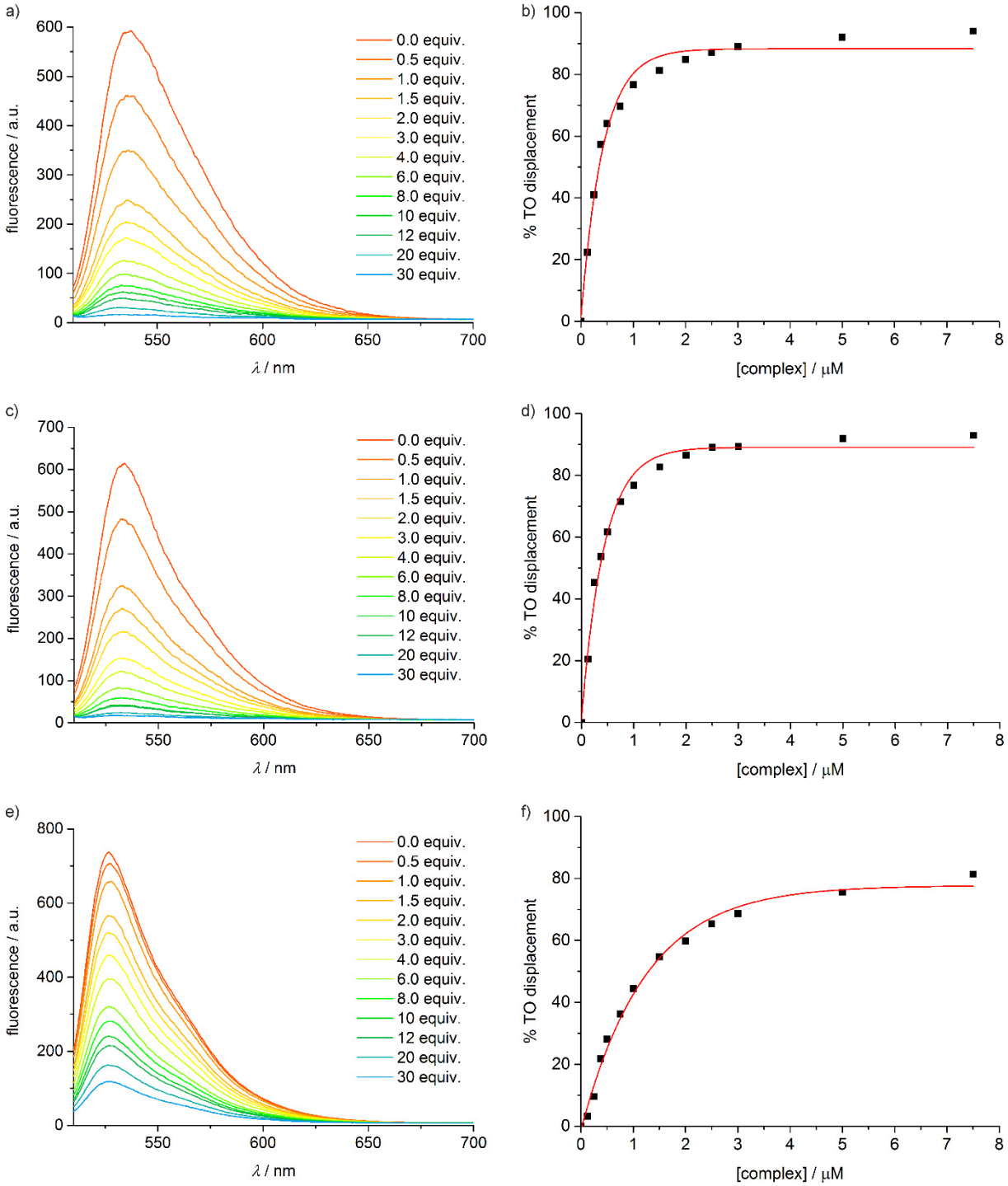

Fig. S25. Fluorescence spectra of TO intercalated into a) H-telo, c) *c-myc* and e) ds26 in the presence of increasing amounts of [Pd(**2p**)Cl] as well as percentage TO displacement from b) H-telo, d) *c-myc* and f) ds26. Experimental details: 0.25 μM oligonucleotide, TO (0.5 μM for quadruplex DNA, 0.75 μM for ds26), 60 mM KCl, 5 mM MOPS (pH 7.4), 0 → 7.5 μM [Pd(**2p**)Cl], 1 cm optical path length. Prior to the titration, 2 μL of DMSO were added to the *c-myc* solution.

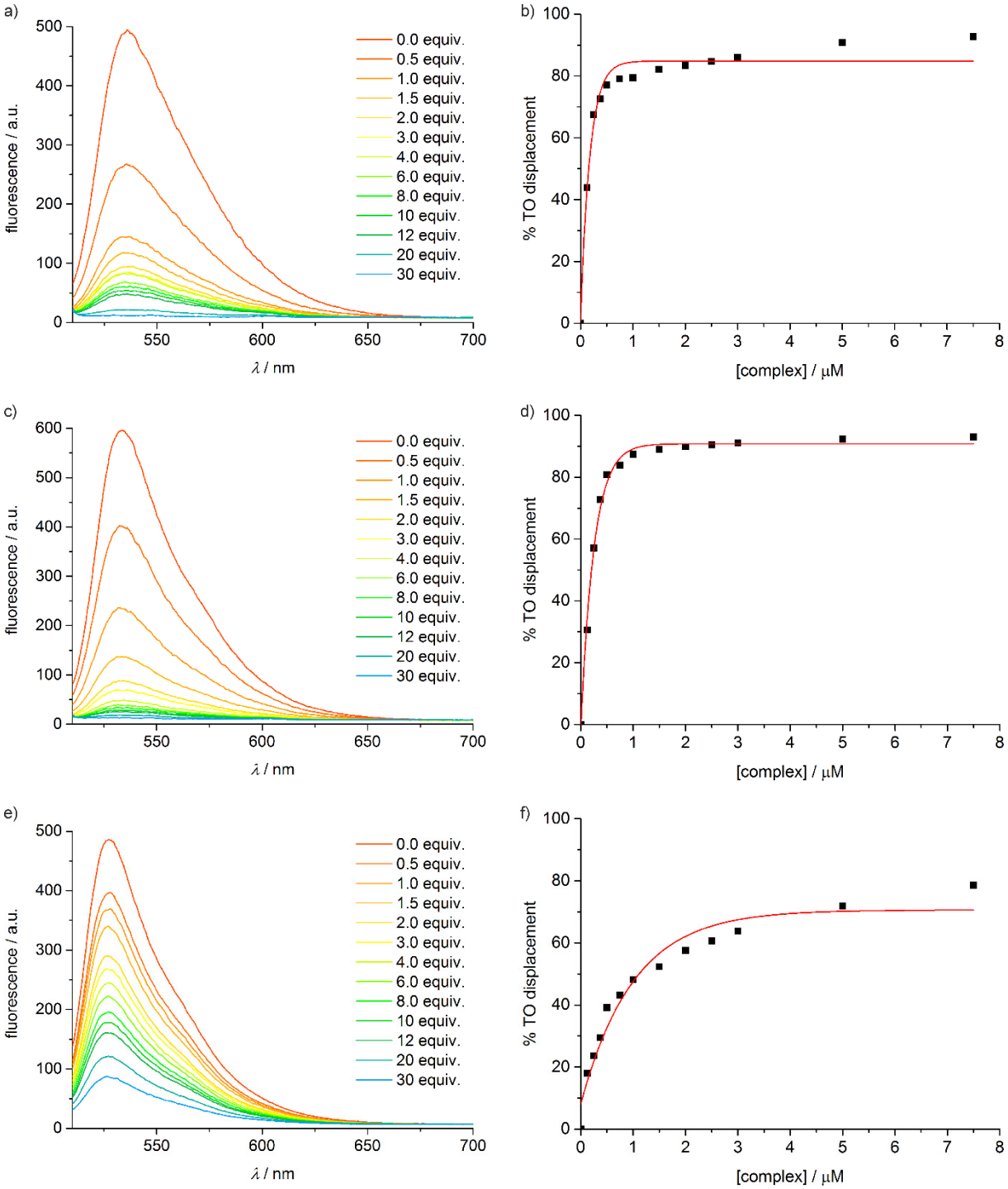

Fig. S26. Fluorescence spectra of TO intercalated into a) H-telo, c) *c-myc* and e) ds26 in the presence of increasing amounts of [Pd(**2q**)Cl] as well as percentage TO displacement from b) H-telo, d) *c-myc* and f) ds26. Experimental details: 0.25 μM oligonucleotide, TO (0.5 μM for quadruplex DNA, 0.75 μM for ds26), 60 mM KCl, 5 mM MOPS (pH 7.4), 0 → 7.5 μM [Pd(**2q**)Cl], 1 cm optical path length. Prior to the titration, 2 μL of DMSO were added to the *c-myc* solution.

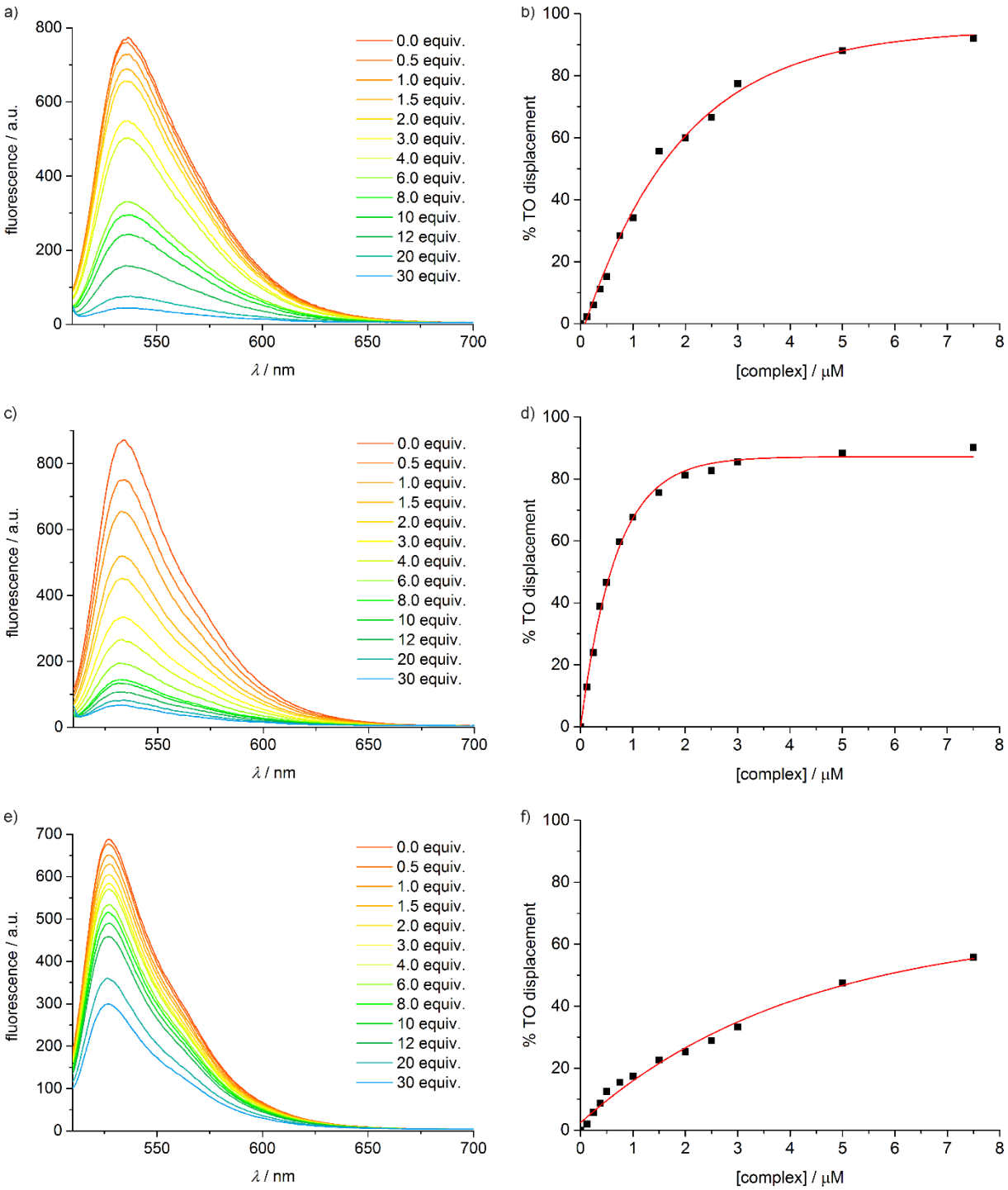

Fig. S27. Fluorescence spectra of TO intercalated into a) H-telo, c) *c-myc* and e) ds26 in the presence of increasing amounts of [Pd(**3q**)Cl] as well as percentage TO displacement from b) H-telo, d) *c-myc* and f) ds26. Experimental details: 0.25 μM oligonucleotide, TO (0.5 μM for quadruplex DNA, 0.75 μM for ds26), 60 mM KCl, 5 mM MOPS (pH 7.4), 0 → 7.5 μM [Pd(**3q**)Cl], 1 cm optical path length. Prior to the titration, 2 μL of DMSO were added to the *c-myc* solution.

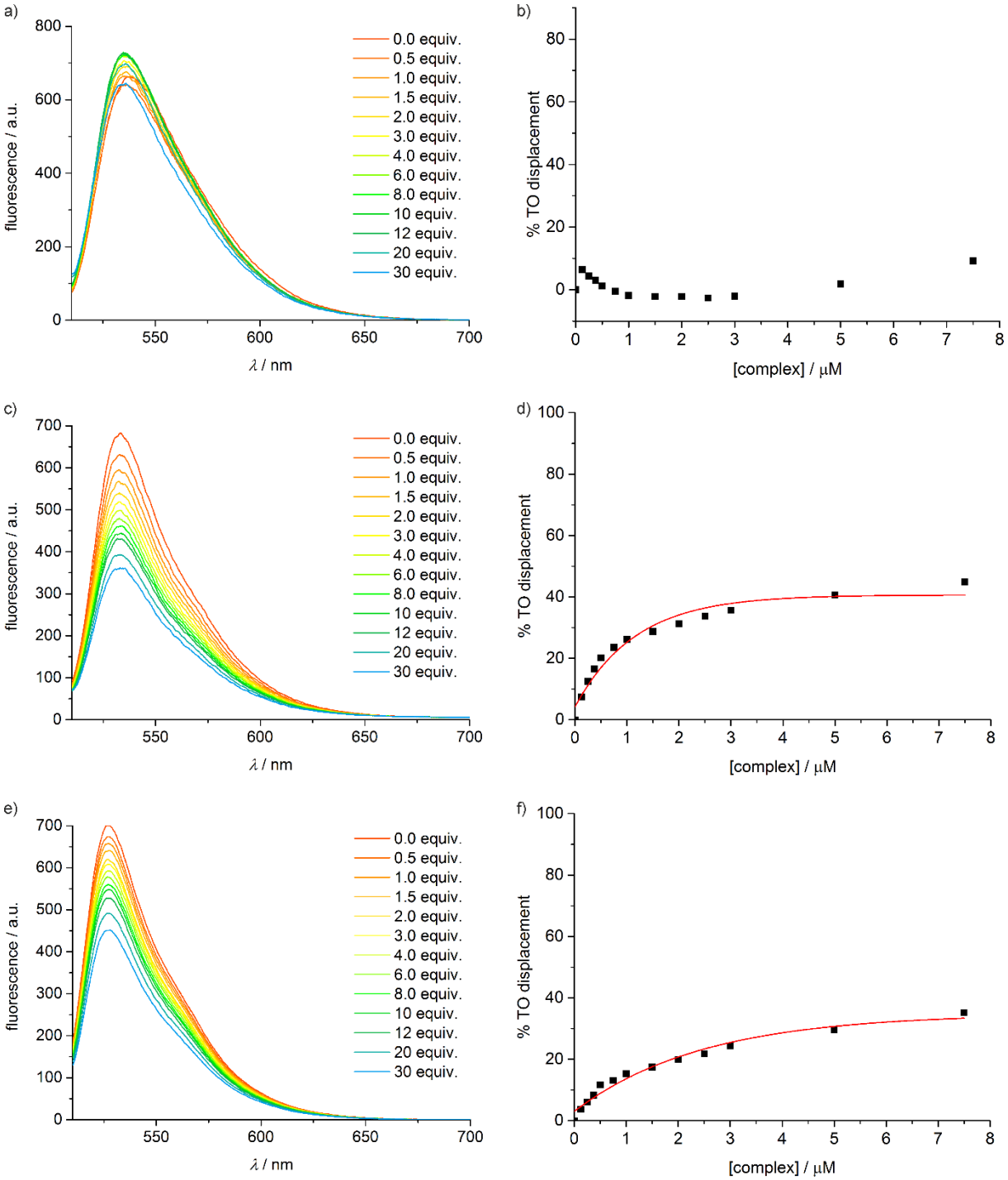

Fig. S28. Fluorescence spectra of TO intercalated into a) H-telo, c) *c-myc* and e) ds26 in the presence of increasing amounts of [Pt(**3q**)Cl] as well as percentage TO displacement from b) H-telo, d) *c-myc* and f) ds26. Experimental details: 0.25 μM oligonucleotide, TO (0.5 μM for quadruplex DNA, 0.75 μM for ds26), 60 mM KCl, 5 mM MOPS (pH 7.4), 0 → 7.5 μM [Pt(**3q**)Cl], 1 cm optical path length. Prior to the titration, 2 μL of DMSO were added to the *c-myc* solution.

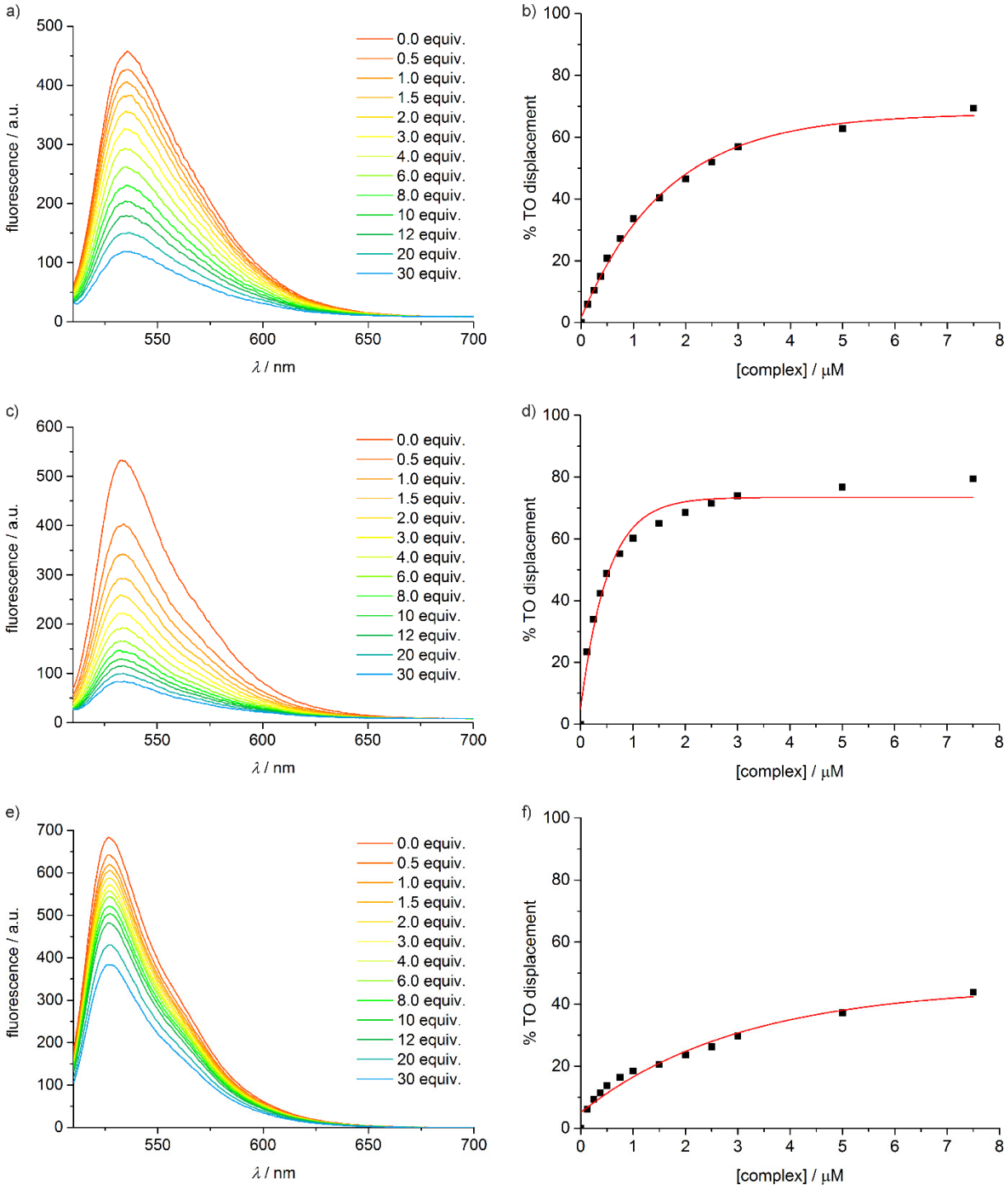

Fig. S29. Fluorescence spectra of TO intercalated into a) H-telo, c) *c-myc* and e) ds26 in the presence of increasing amounts of [Pt(**4q**)Cl] as well as percentage TO displacement from b) H-telo, d) *c-myc* and f) ds26. Experimental details: 0.25 μM oligonucleotide, TO (0.5 μM for quadruplex DNA, 0.75 μM for ds26), 60 mM KCl, 5 mM MOPS (pH 7.4), 0 → 7.5 μM [Pt(**4q**)Cl], 1 cm optical path length. Prior to the titration, 2 μL of DMSO were added to the *c-myc* solution.

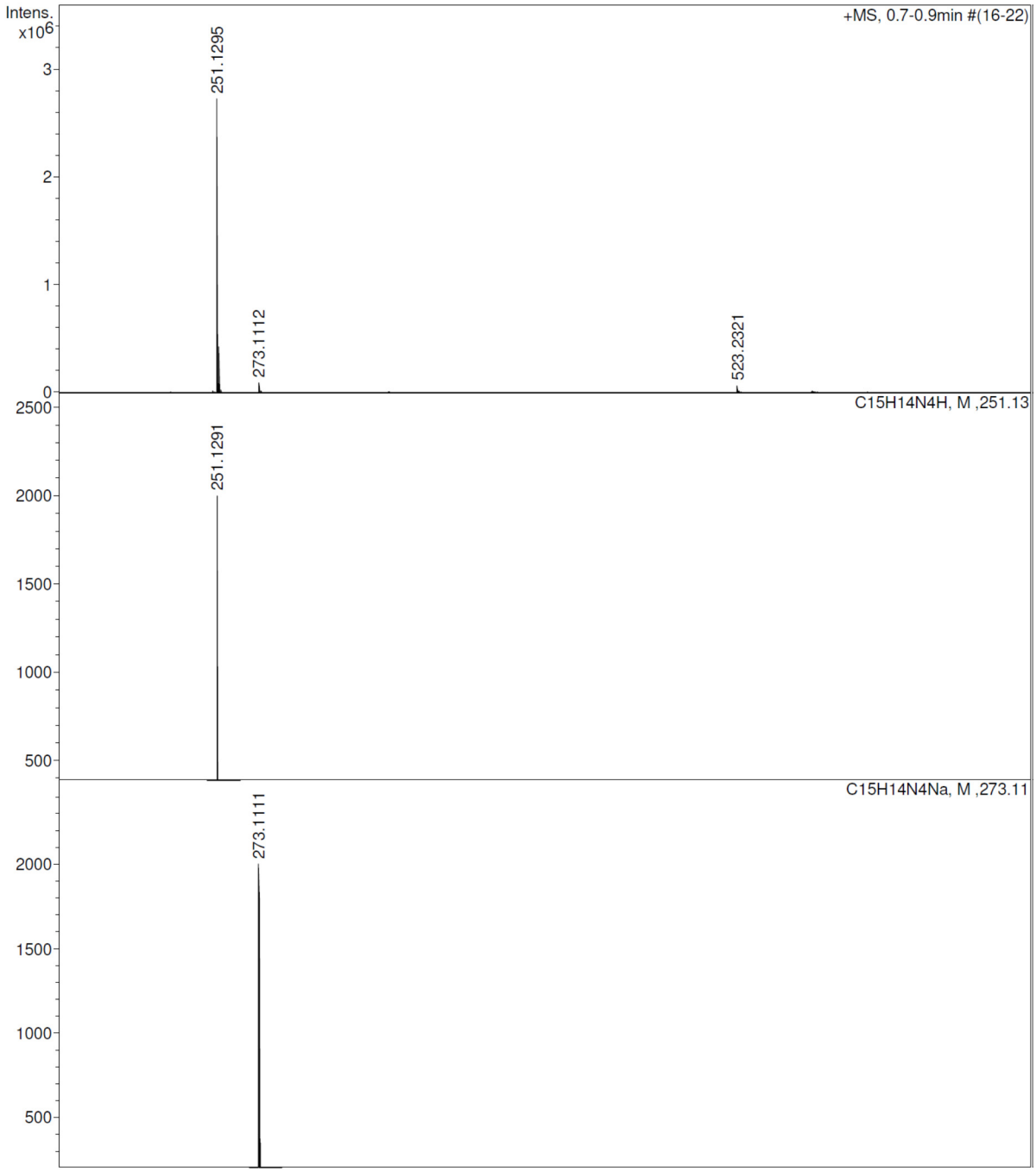

Fig. S30. ESI-TOF mass spectrum of H(**2q**). Top panel: experimental spectrum; middle panel: spectrum calculated for $[M + H]^+$; bottom panel: spectrum computed for $[M + Na]^+$.

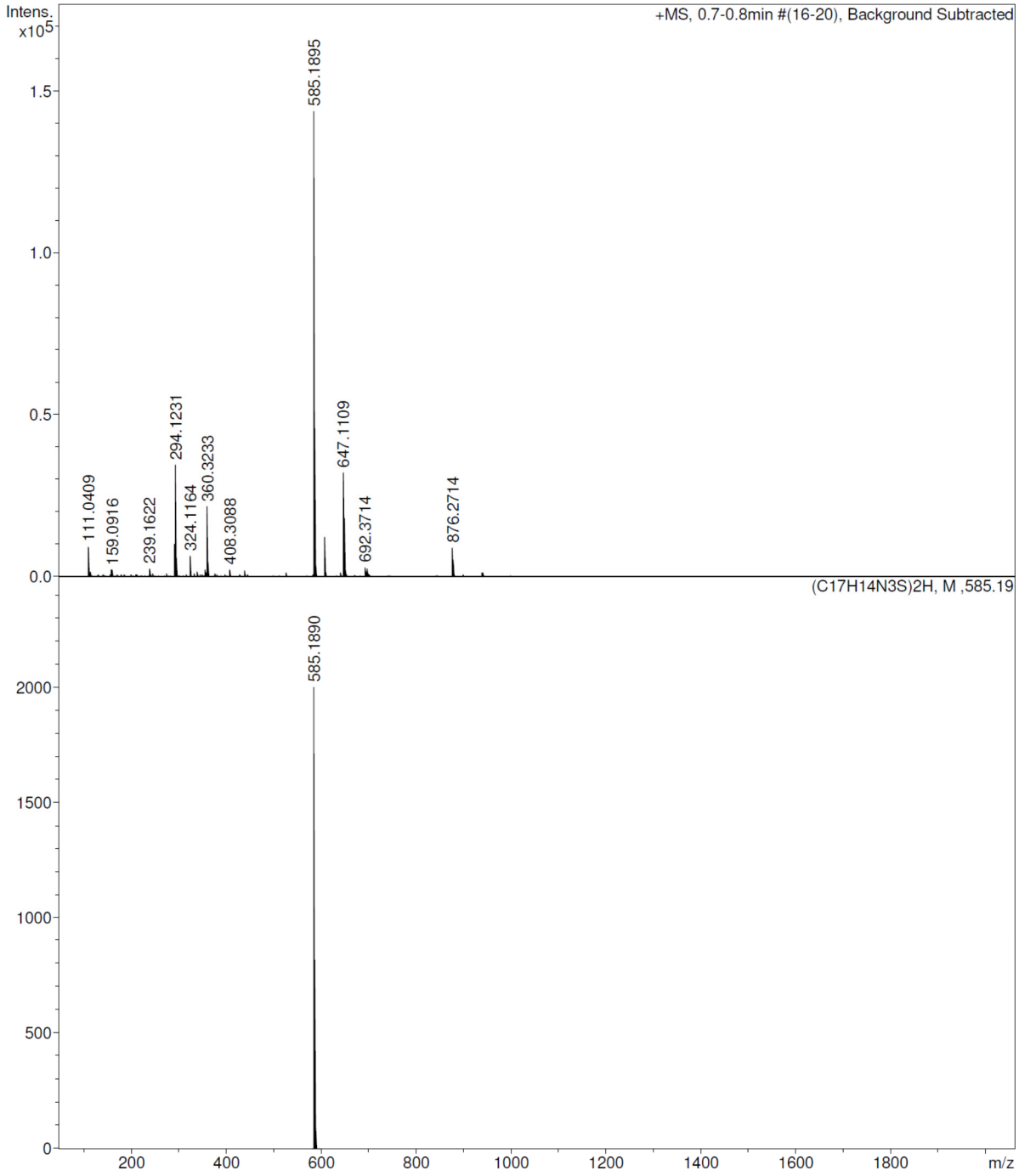

Fig. S31. ESI-TOF mass spectrum of H(**3q**). Top panel: experimental spectrum; bottom panel: spectrum computed for $[2M + H]^+$.

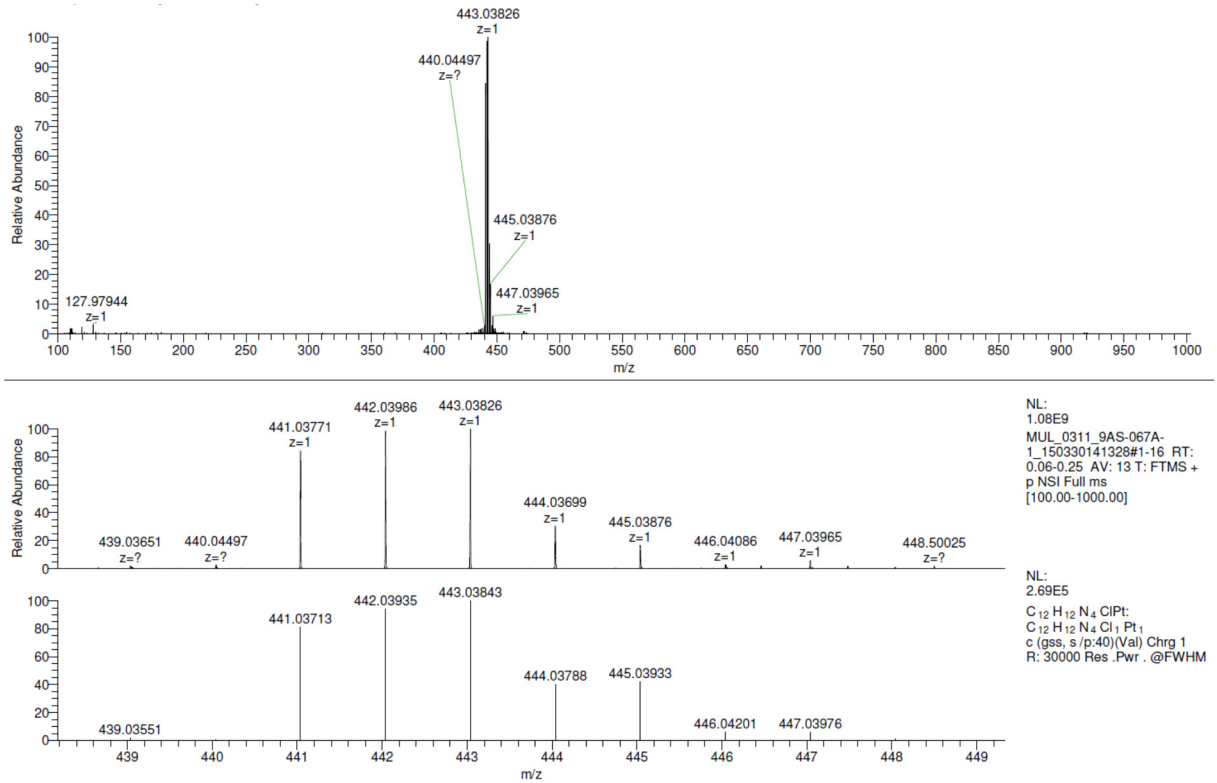

Fig. S32. ESI-MS spectrum of [Pt(**1p**)Cl]Cl. Top panel: experimental spectrum; bottom panels: excerpt of the experimental spectrum and spectrum computed for $[M - Cl]^+$.

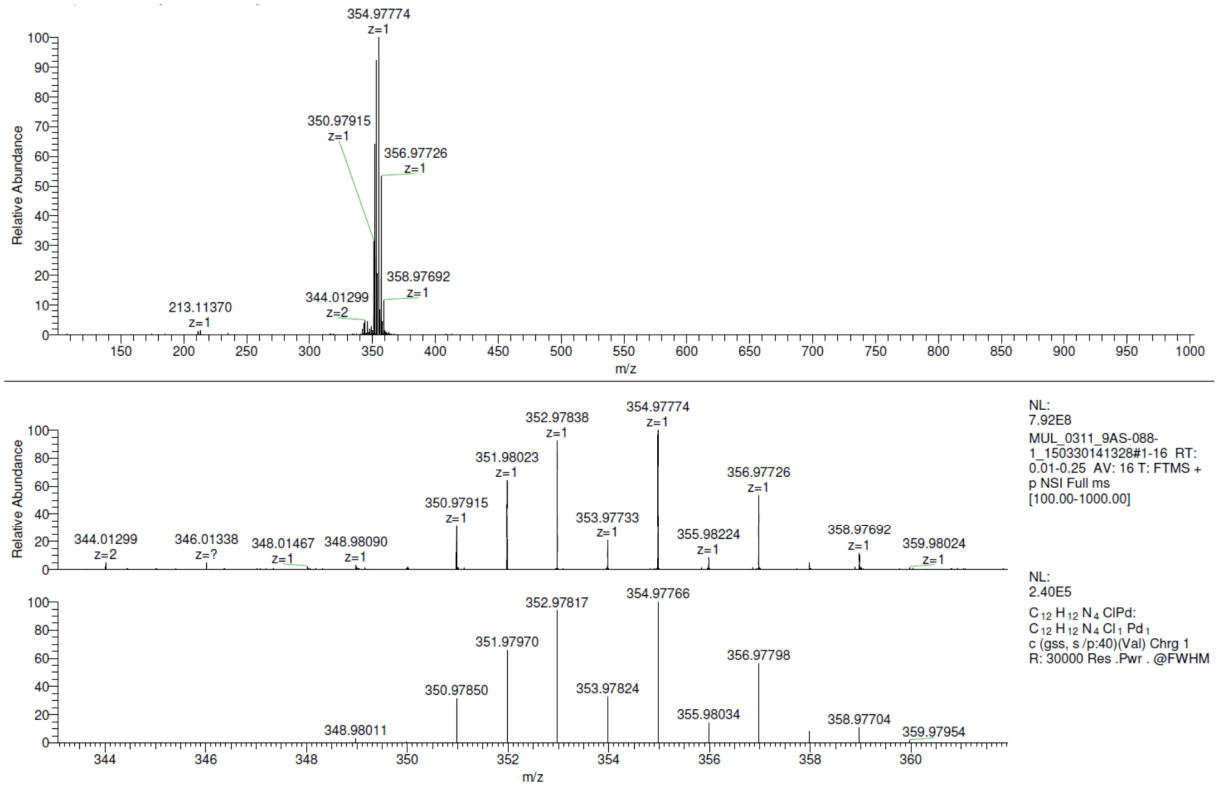

Fig. S33. ESI-MS spectrum of [Pd(**1p**)Cl]Cl. Top panel: experimental spectrum; bottom panel: excerpt of the experimental spectrum and spectrum computed for $[M - Cl]^+$.

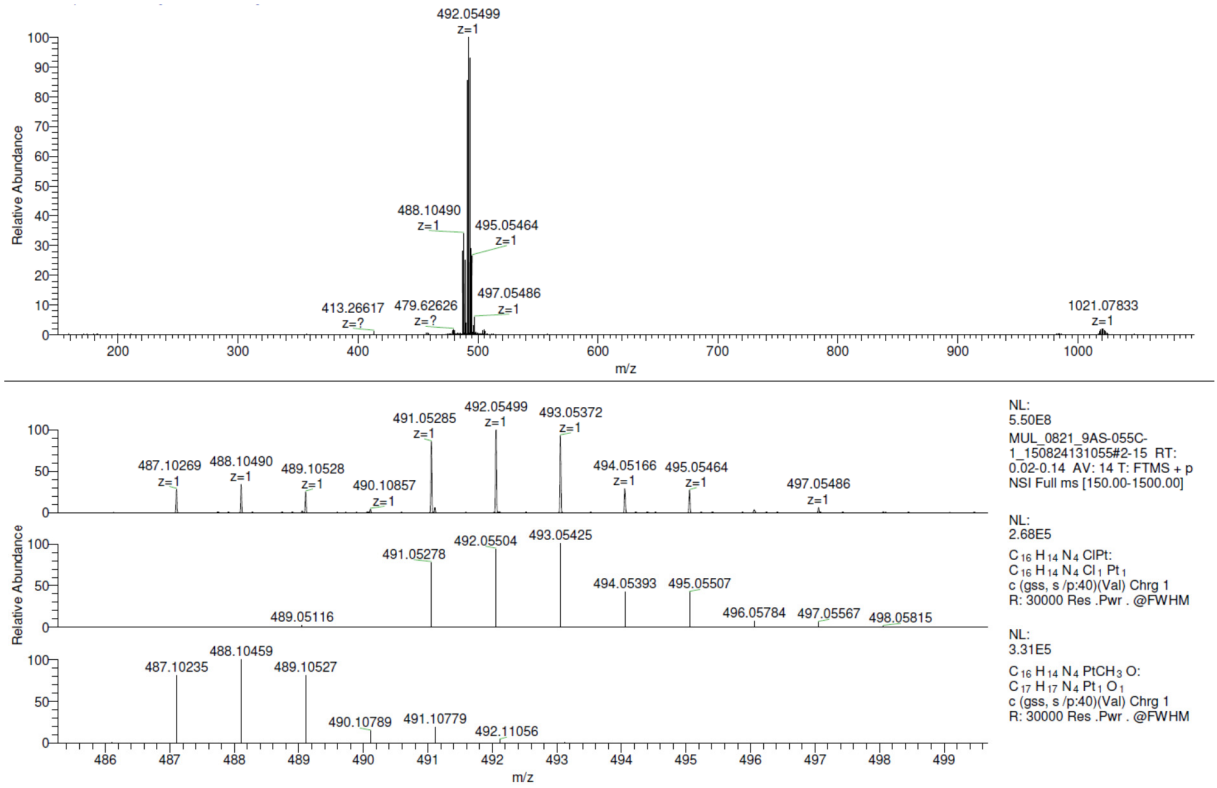

Fig. S34. ESI-MS spectrum of [Pt(**1q**)Cl]Cl. Top panel: experimental spectrum; bottom panel: excerpt of the experimental spectrum and spectra computed for $[M - Cl]^+$ and $[M - 2Cl + OCH_3]^+$.

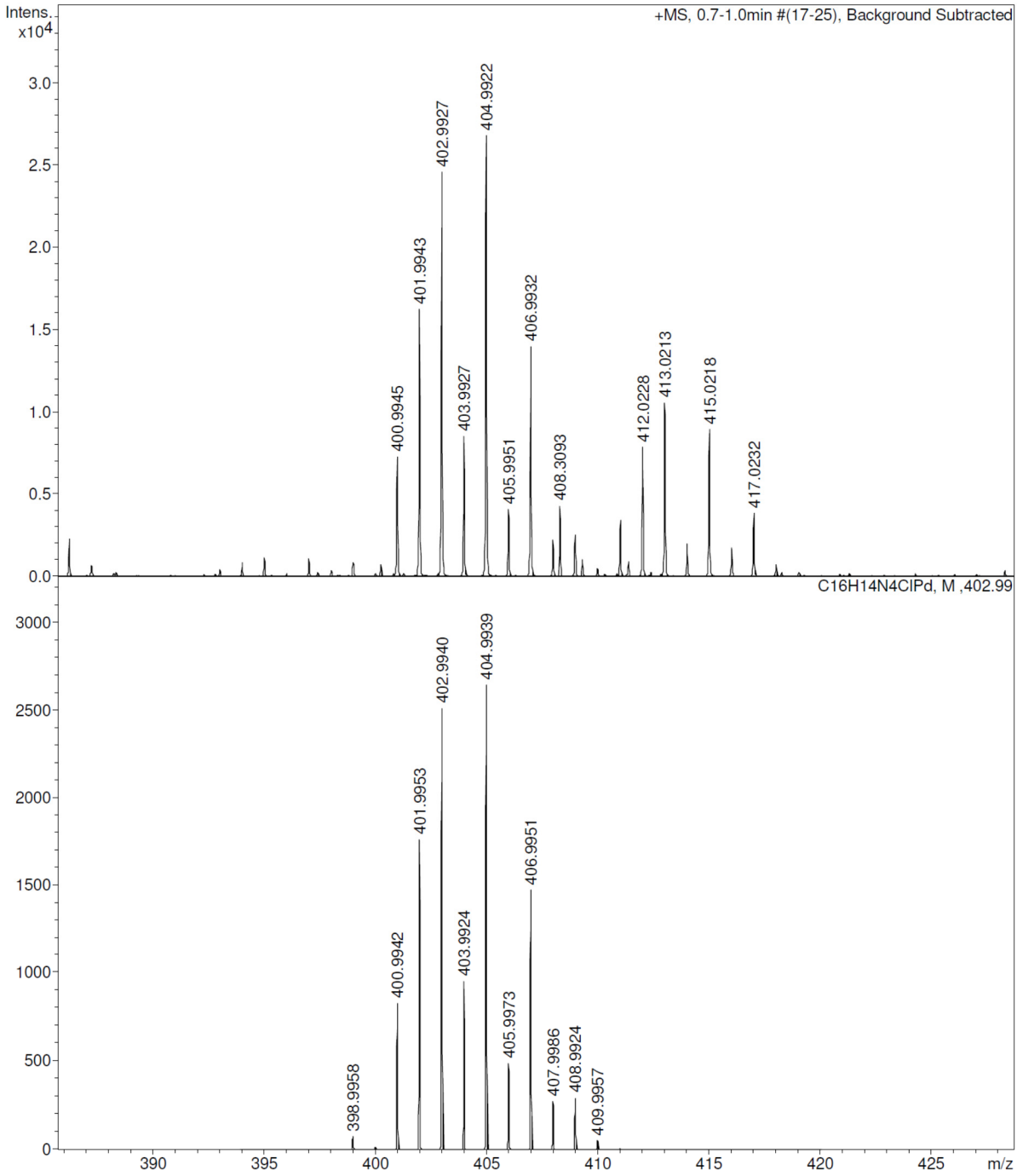

Fig. S35. ESI-TOF mass spectrum of [Pd(**1q**)Cl]Cl. Top panel: excerpt of the experimental spectrum; bottom panel: spectrum computed for $[M - Cl]^+$.

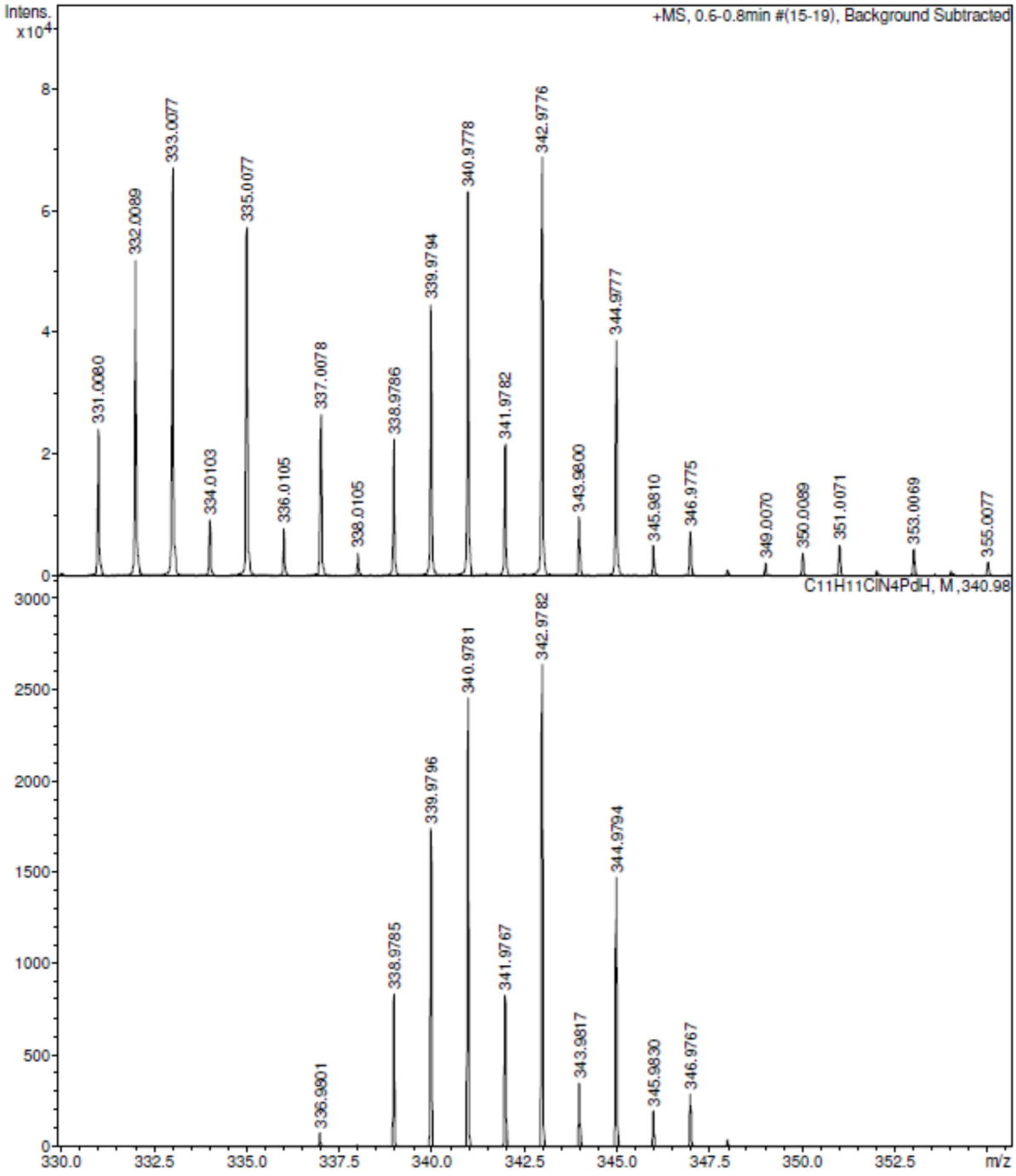

Fig. S36. ESI-TOF mass spectrum of [Pd(**2p**)Cl]. Top panel: excerpt of the experimental spectrum; bottom panel: spectrum computed for $[M + H]^+$.

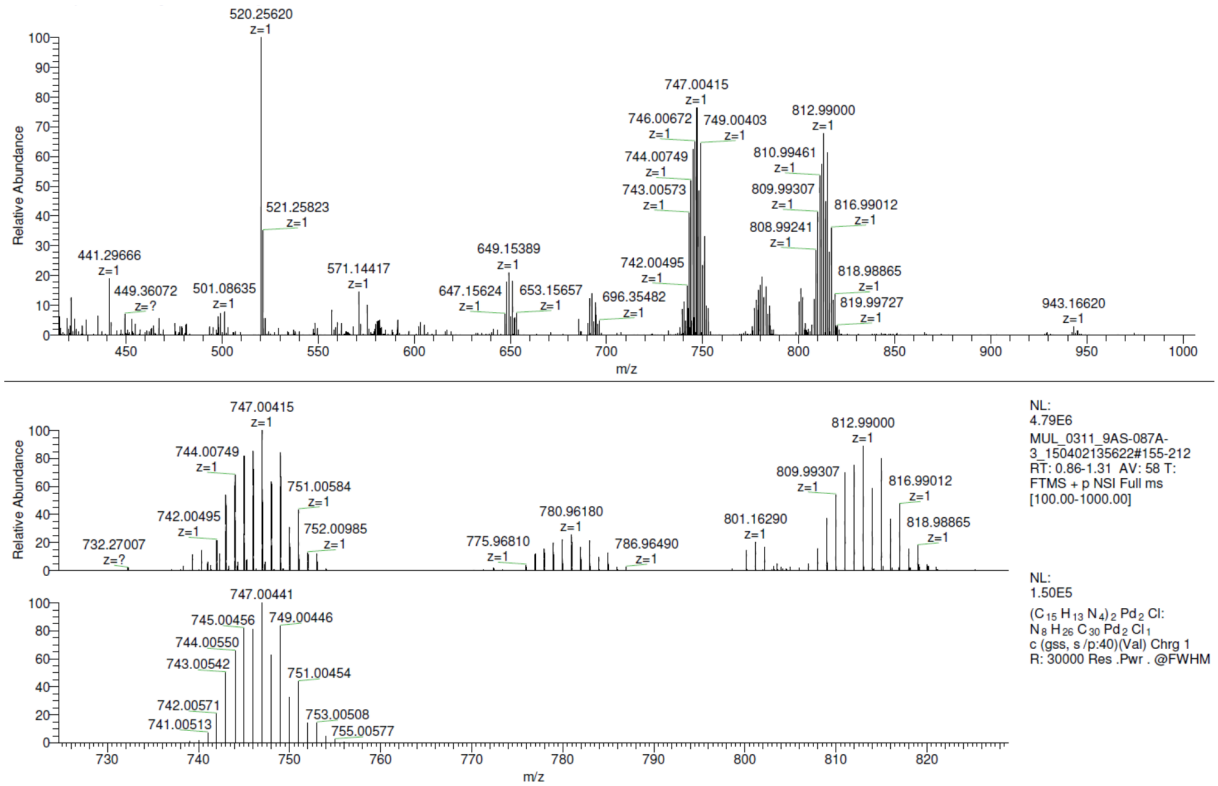

Fig. S37. ESI-MS spectrum of [Pd(**2q**)Cl]. Top panel: experimental spectrum; bottom panel: excerpt of the experimental spectrum and spectrum computed for $[2M - Cl]^+$.

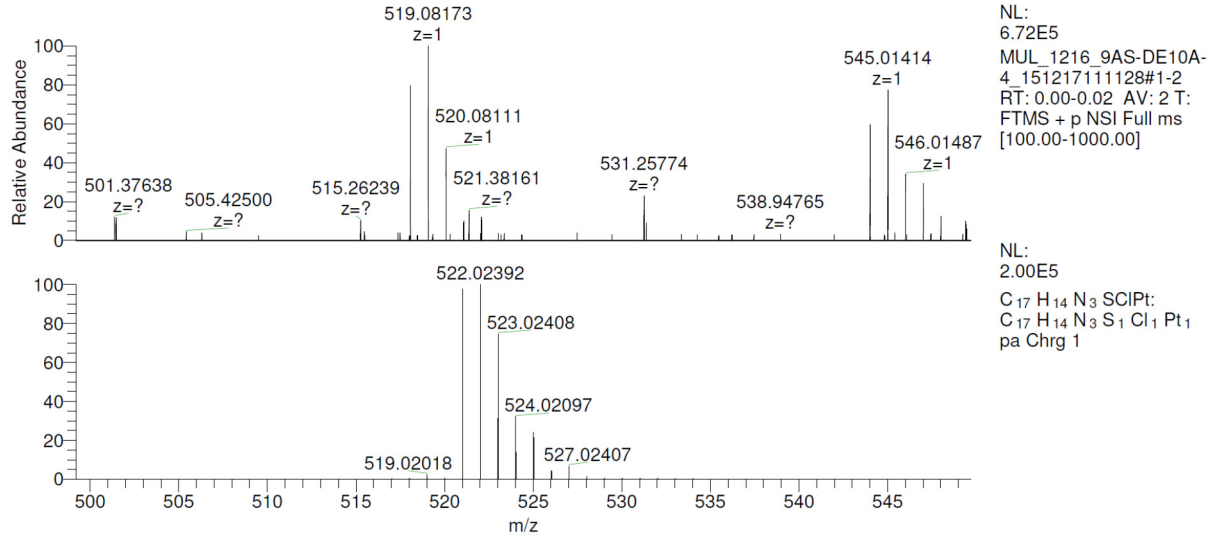

Fig. S38. ESI-MS spectrum of [Pt(**3q**)Cl]. Top panel: excerpt from experimental spectrum; bottom panel: spectrum computed for $[M]^+$, the experimental peaks around m/z = 545 have not been plotted in the computed spectrum but can be assigned to $[M + Na]^+$, as they show the correct isotopic pattern of the product peak.

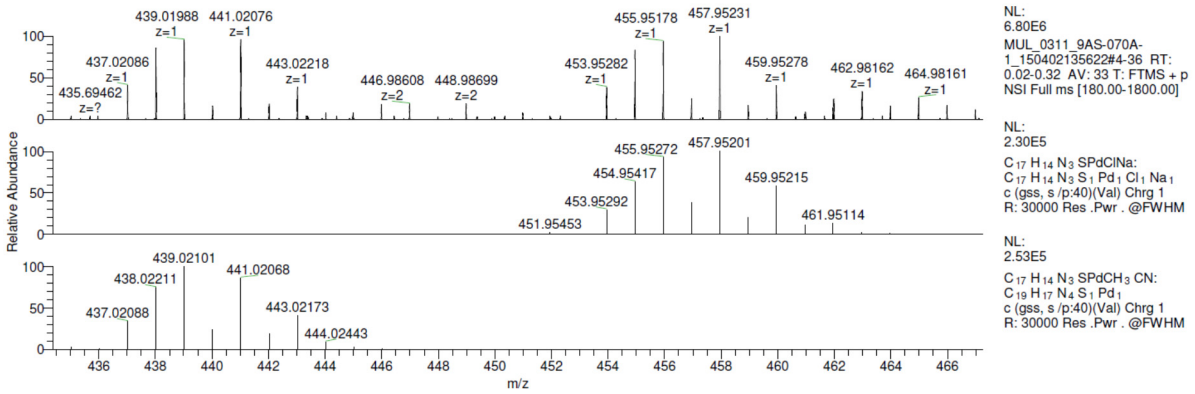

Fig. S39. ESI-MS spectrum of [Pd(**3q**)Cl]. Top panel: excerpt of experimental spectrum; bottom panels: spectra computed for $[M + Na]^+$ and $[M - Cl + CH_3CN]^+$.

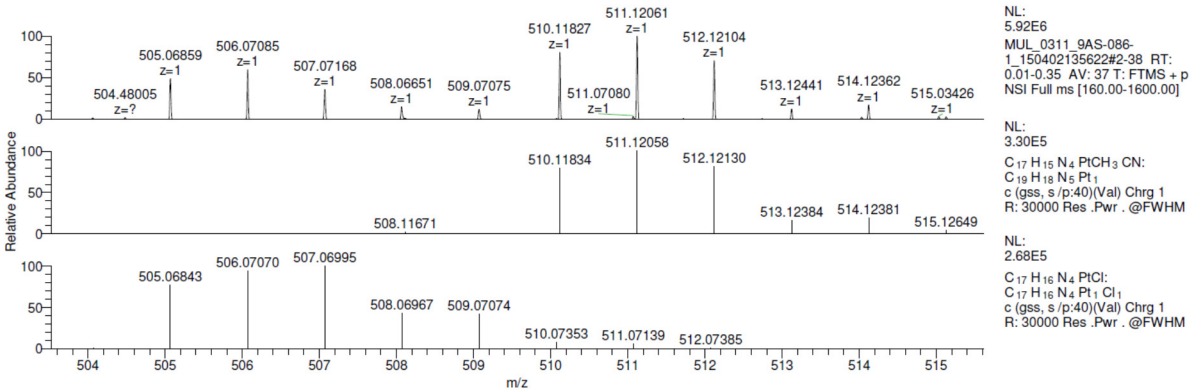

Fig. S40. ESI-MS spectrum of [Pt(**4q**)Cl]. Top panel: excerpt of experimental spectrum; bottom panels: spectra computed for $[M - Cl + CH_3CN]^+$ and $[M + H]^+$.